MOLECULAR DYNAMICS SIMULATIONS OF LASER SPIKE ANNEALING OF BLOCK COPOLYMER THIN LAMELLAR FILMS

A Thesis

Presented to the Faculty of the Graduate School

of Cornell University

In Partial Fulfillment of the Requirements for the Degree of

Master of Science

by

Chih-Yin Chen

August 2018

ABSTRACT

Recent experimental studies have reported that laser spike annealing (LSA) can accelerate the order-disorder transition “ODT” (for melting and reordering) of block copolymer thin films. With LSA the polymer is subjected to much higher temperatures but for a far shorter time compared to traditional thermal annealing, resulting in an induced disordering temperature that increases as the heating/cooling cycle decreases. Such a trend arises from the LSA time scale being shorter than the time scale for the ODT at the thermodynamic ODT temperature, but longer than the polymer relaxation time scale. In this work, we use molecular dynamic simulations of a simple coarse-grained model to study the phase behavior of a general lamella-forming A-b-B di-block copolymer thin film under different heating cycle lengths, film thickness, and substrate-polymer affinity. This model describes a realistic soft confinement scenario to study the effects of a free surface (air-polymer interface) and solid substrate selectivity on thin film morphology. Our simulation results successfully capture a similar trend for the ODT temperature as in LSA experiments (for comparable heating cycle lengths) when the vertical lamella phase formed on neutral substrates. In addition, simulations with a substrate selective for a particular block revealed the formation of a metastable island phase having horizontal but incomplete lamella layers. The nanoscale roughness features of this island phase could be of potential use to modulate the wettability of surfaces as the degree of roughness can be controlled to some extent with suitable choices of polymer chemistry and the annealing conditions.

BIOGRAPHICAL SKETCH

Chih-Yin Chen was born in Taipei, Taiwan in the year 1992. During his undergraduate study at National Taiwan University, he double majored in chemical engineering and finance. He received a Bachelor of Science and a Bachelor of Business Administration in 2015. He started his graduate study to pursue a Master of Science degree at Cornell University and worked on his research under the supervision of Prof. Fernando A. Escobedo in 2016.

ACKNOWLEDGMENTS

I would first like to thank my thesis advisor, Prof. Fernando A. Escobedo. His passion and wisdom have led me through my journey of research. He always welcomes me to ask any question about research and writing. Without his support and guidance, this accomplishment would not have been possible.

I would like to thank my thesis committee, Prof. Yong L. Joo for insightful suggestions throughout this project. He is also willing to help me with any question I had during my study at Cornell as the director of Master of Science program.

I would like to thank Prof. Michael Thompson and Dr. Alan Jacobs for providing experiment details and useful discussions that helped me bridge the gap between the experiment and the simulation.

I would also like to thank Escobedo group members, Dr. Mayank Misra, Christian Nowak, Prajwal B. P., Yangyang Sun and Mohammed AlShammasi for inspirational discussion and guidance toward molecular simulation.

Finally, I would also like to thank my parents for their wise counsel and unfailing encouragement throughout my years of graduate study.

TABLE OF CONTENTS

CHAPTER 1

INTRODUCTION

1.1 Block Copolymers Self-Assembly

Block copolymers (BCPs) combine two or more chemically distinct blocks covalently attached into a single polymer chain. BCPs self-assemble into nanoscale morphologies through phase segregation and ordering mechanisms that reflect a complex interplay of thermodynamics and kinetic effects [1-3]. This BCP self-assembly ordering presents wide applications ranging from directed self-assembly (DSA) lithography [4], bit patterned media [5], filters [6], fuel cell membranes [7], drug delivery vectors [8] and adhesives [9].

The bulk BCP phase segregation and self-assembly process has been studied both experimentally [10] and theoretically [11][12]. The equilibrium phase behavior of A-b-B di-block copolymers (dBCP) provides a variety of ordered structures, depending on the Flory-Huggins segment-segment interaction parameter χ, the polymer chain length N, and the monomer volume fraction of polymer type A f_A. Theoretically, the Flory-Huggins parameter is inversely proportional to temperature [11]. When temperature is higher than the order-disorder temperature (T_{ODT}), the product χN is lower than the critical point ($\chi N < 10.5$ for infinitely long chain [13] with $f_A = 0.5$) and the blocks mix into a disorder phase. Conversely, phase segregation happens when cooling the disordered system below T_{ODT}, where depending on BCP

composition different ordered phases are formed to minimize the interaction between A and B blocks. A global phase diagram is shown in Figure 1 [14]. Upon increasing the volume fraction of polymer A from f_A = 0 to 0.5, the ordered structures transition from cubic-packed spheres through hexagonally packed cylinders, bicontinuous gyroid networks and lamellar sheets. The processes of phase segregation and structure formation are crucial to the generation of morphologies useful for applications.

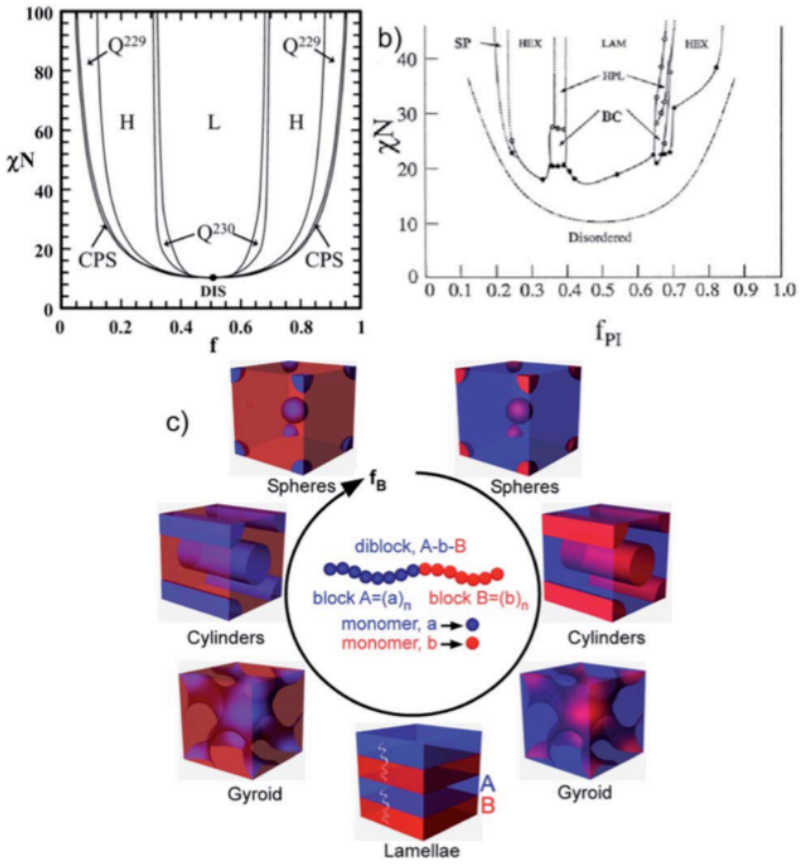

Figure 1. Bulk phase behavior of diblock copolymer. Adapted from ref. 14.

BCP thin films are also of interest because of the growing potential of nano-patterned devices and photonic applications [15]. The surfaces in contact with the thin film act to spatially confine the material and can modify the bulk phase behavior and ordering kinetics [45]. Two types of confinements are widely used for BCPs thin films: hard or soft confinement [16][41]. In hard confinement, the thin film is confined between two rigid interfaces. In soft confinement describes one of the surfaces is free (the air-polymer interface) and the other is a solid substrate. Many studies have been focused on controlling the thin film morphology under these confinements via directed self-assembling (DSA) techniques to achieve the desired structures, such as thermal annealing [17], vapor annealing [18], and chemically patterned substrate [19]. Henceforth we only consider soft confinement.

The orientation of the ordered structure of an A-b-B diblock copolymer (dBCP) thin film is highly sensitive to substrate wetting [36][37]. For a symmetric dBCP and a neutral substrate that has a similar attraction to both polymer bead A and bead B, the equilibrium order phase will be a lamella phase with layers aligned vertically to the substrate. If the substrate attraction is selective to favor bead A or bead B, the equilibrium order phase will be a lamella phase with layers parallel to the substrate, with the bottom layer being of the favored bead. Moreover, a peculiar island phase has been found for horizontally aligned lamella phase with non-perfect layers open to the air-polymer interface [38-43]. Lastly, a hybrid lamella phase, which contains both vertically and horizontally aligned lamella, has been found experimentally for certain thicknesses of the thin film and vapor annealing conditions [44].

While the typical thermal annealing time scale is from minutes to hours (e.g., using vacuum oven annealing) [17], Jacobs *et al.* employed laser spike annealing (LSA) to study the order-disorder transition of dBCPs[20][21]. The order-disorder transition can be accelerated far in excess of that achievable by thermal equilibrium by using sub-millisecond lateral gradient LSA where the polymer experiences much higher temperatures but for a far shorter time. Indeed, by heating the sample up to temperatures far above T_{ODT} for a millisecond time duration, Jacobs *et al.* explored the effect of a previously inaccessible thermal region on the kinetics of the phase segregation process. They also showed that the final structure after laser annealing depends on both annealing temperature and quenching rate, as shown in Figure 2.

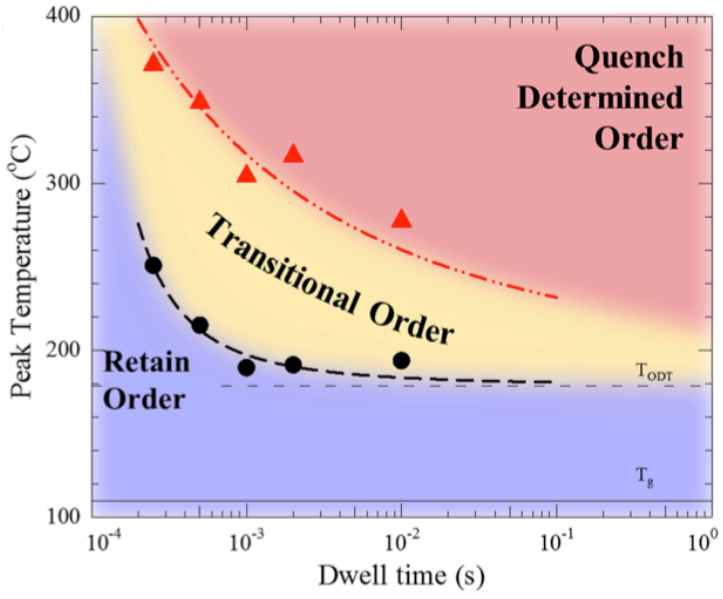

Figure 2. dBCP phase map after LSA, showing how the final structure depends on the annealing time and peak temperature. Adapted from ref. 21.

1.2 Molecular Simulation

Modeling studies can help elucidate the mechanism of order-disorder transitions of BCP systems under different processing conditions. However, most of the simulation studies have focused on bulk BCPs phase segregation behavior. Furthermore, most of the simulations of BCP thin film morphologies have dealt with hard confinement [22][23] or a freestanding polymer film (i.e., having two air-polymer interfaces and no substrate) [24][25]. On the other hand, very few modeling studies have explored soft confinement and the effects of a free surface (air-polymer interface) and solid substrate selectivity on thin film morphology.

Forrey *et al*. employed a simple coarse-grained model and molecular dynamics simulation to study soft confinement of dBCPs [26][27]. They have shown that by controlling annealing temperature and substrate preference to different type of polymers, different orientation of lamellae phase (vertical or horizontal to the substrate) can be created, including defective island phases.

In this work, we seek to apply a coarse-grained model to simulate the phase behavior of a general A-b-B dBCP thin film under a soft confinement. Our main goal is to understand the effect on the order-disorder transitions via a fast heating-cooling protocol that mimics laser annealing. The ordering and disordering mechanisms of the thin film is tested by using different heating and cooling rates as well as different peak heating temperatures (below and above T_{ODT}) as was done with laser annealing. Different substrate preferences are also tested to understand the effect of substrate wetting. By controlling the cooling rate, we found that island phase is formed not only

during the heating process as Forrey *et al.* [26] previously showed, but also by "retreating" from a perfect horizontal lamella phase when cooling to low temperature. Also, we seek to understand factors that control the formation of the island phase, as a strategy to create a surface with nanoscale roughness for such potential application as the engineering of super-hydrophobic surfaces.

The rest of this manuscript is organized as follows. Chapter 2 describes the coarse-grained model adopted, details of simulation methods implemented, and the order parameters used to characterize the morphologies. Chapter 3 summarizes the phase behavior of dBCP thin films at different temperatures and upon annealing with different heating and cooling rates. Finally, Chapter 4 presents our conclusions.

CHAPTER 2

SIMULATION METHODOLOGY

2.1 Simulation Protocols and Molecular Model

2.1.1 dBCP Thin Film Simulation

We adopt a simple coarse-grained model to study the phase behavior of a general A-b-B dBCP thin film, following the work of Forrey *et al* [26]. A general A-b-B dBCP is composed of two chemically distinct coarse-grained beads, type A and type B. The difference in attraction between A and B beads provides a significant variation in the air-polymer surface tension which also affects the thin film morphology.

While this model is suitable to study the morphology of dBCP thin films, it is important to select molecular weights that would allow studying the order-disorder transition above T_{ODT}, where evaporation can occur. Small chain lengths are convenient from a computational perspective as they equilibrate fast, but could evaporate at temperatures close to the T_{ODT}. As a compromise we chose a polymer chain with a moderate chain length, i.e., the linear polymer chain is composed with twenty beads, with equal number of A and B (10:10) beads to study the lamella morphology, as shown in Figure 3. Note also that the attraction of the polymer to the substrate provides additional stability to the thin film structure even at higher temperatures.

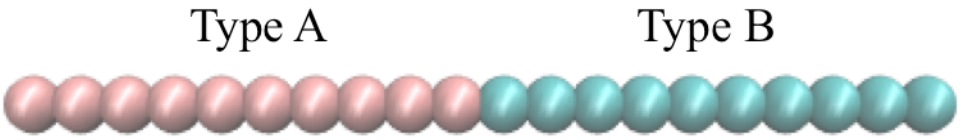

Figure 3. Coarse-grained dBCP chain, all beads are the same diameter, σ, and mass.

Each dBCP coarse-grained bead represents a group of chemical units. Bonded interactions act only between bonded beads in the same chain and constrain their separation distance by a harmonic potential of the form

$$U_{bond}^{harmonic}(r) = \frac{1}{2}K_{spring}(r - r_0)^2 \quad (1)$$

where r is the separation distance between the bonded beads, r_0 is the equilibrium separation, and K_{spring} is the spring constant.

Non-bonded interactions are determined by pairwise Lennard-Jones potentials including an attractive tail between all bead types

$$U_{ij}^{LJ}(r) = 4\varepsilon_{ij}\left[\left(\frac{\sigma_{ij}}{r}\right)^{12} - \left(\frac{\sigma_{ij}}{r}\right)^{6}\right], r < 3\,\sigma_{ij} \quad (2)$$

where i and j represent the bead type, r is the bead separation, ε_{ij} is the depth of the potential well, σ_{ij} is the distance where the inter-particle potential is zero. A type beads are tuned to have higher self-attraction than B type beads while the attraction between A and B beads is even weaker to drive phase segregation. Unlike the commonly used Kremer-Grest bead spring model [28], in which the potential between dissimilar beads is purely repulsive (known as Weeks-Chandler-Andersen reference system potential [29]), here we use an attractive tail between all bead types to ensure

film cohesion, which is necessary when having a free surface.

The parameters used in this model are presented in Table 1. All units are presented in LJ reduced units, $T^* = TK_B/\varepsilon$, where K_B is Boltzmann's constant, and pressure, $P^* = P\sigma^3/\varepsilon$, length, $L^* = L/\sigma$, time, $\tau = t(\varepsilon/m\sigma^2)^{0.5}$. However, for temperatures we will use reduced temperatures defined as $T_r = T^*/T_{ODT}$, where T_{ODT} is the order-disorder temperature (ODT) for the bulk system in LJ units, which is taken to be $T_{ODT} = 2.8$ based on our bulk phase simulation results (see Section 3.1).

Table 1. Simulation parameters

Type	Parameter	Value
Bond stretching	r_0	1
	K_{spring}	500
Lennard-Jones interaction	ε_{AA}	1.9
	ε_{BB}	1.6
	ε_{AB}	0.8
	$\varepsilon_{substrate\ (neutral)}$	3.5
	$\varepsilon_{substrate\ to\ favored\ bead}$	4.5
	$\varepsilon_{substrate\ to\ unfavored\ bead}$	0.75
	$\varepsilon_{substrate\ to\ substrate}$	0
	σ_{ij}	0.84

Note also that the Lennard-Jones interaction parameter ε_{AA} (= 1.9) is set to be

higher than ε_{BB} (= 1.6) to satisfy two simulation goals: (1) To provide a driving force for wetting the free surface by the lower surface energy bead B by introducing a difference in cohesive self-interactions of the two blocks. (2) To ensure microphase separation with a positive interaction mismatch parameter, χ, which relates to ε as

$$\chi \sim \frac{-(\varepsilon_{AB} - 0.5(\varepsilon_{AA} + \varepsilon_{BB}))}{K_B T} \quad (3)$$

Simulations were performed via the LAMMPS molecular dynamics (MD) simulation package [30] using a canonical (NVT) ensemble with a reduced time step of 0.005 τ. VMD was used for visualization [31]. The simulation box was 55 x 55 x 70.5 L* in x, y, and z directions. Different system sizes were studied by placing 3000, 4000 or 6000 chains in the system to test the effect of film thickness. 8868 substrate beads were placed below the thin film with hexagonal close-packed arrangement to form two layers of the solid substrate. All substrate beads were immobilized by a harmonic potential (with the same K_{spring} of Table 1) to only allow small fluctuations around their lattice positions; these substrate beads only interact with the polymer beads and not among themselves. Periodic boundary conditions were applied in the xy plane while z direction was made to be non-periodic. Reflective walls were applied at both the lower and upper bounds of the z dimension of the box.

Configurations with locally segregated blocks were obtained following the spin-cast procedure described by Forrey *et al.* [26] and were used as initial configurations for disordered thin films. Simulation runs at $T_r = 0.54$ were performed with different substrates until the lamella phase was formed and then the system was cooled to T* = 1 or $T_r = 0.36$ and maintained at T* = 1 for 10^6 steps to be used as the

initial ordered configurations, as illustrated in Figure 4. We note that for our ensuing discussion the value of T_r = 0.36 will just be referred to as T_0, and is a value representing a very "cold" system, below room temperature but above its glass transition temperature, where any structure can be considered "arrested" or "locked" so that no further significant morphological rearrangements take place.

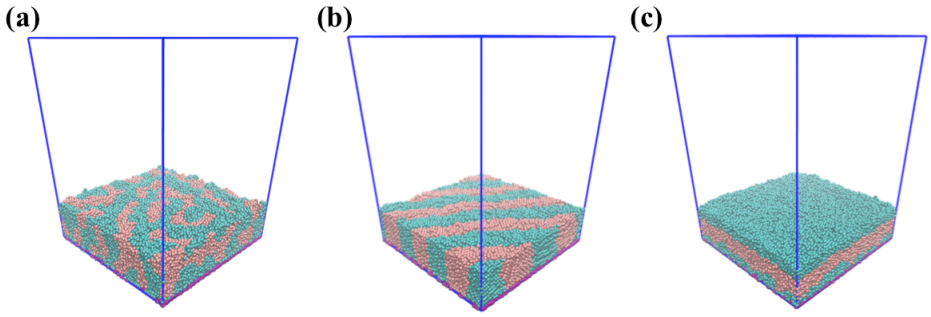

Figure 4. Snapshots of (a) Disordered phase, (b) Vertical lamella phase formed on neutral substrate, and (c) Horizontal lamella phase formed on B-bead selective substrate.

The simulation procedure is illustrated in Figure 5. The simulation system can be considered as a small area of the experimental thin film scanned by the laser. Thus, to simulate the laser annealing experiment, we tested the ordered phase with different ramp periods, namely: 10^5, 10^6, 2×10^6 and 4×10^6 time steps, and with different peak temperature T_{peak} below and above bulk T_{ODT}; namely, from T_r = 0.82 to T_r = 1.18 Each simulation run had a 10^5 steps at T_0 = 0.36 as initial period, and then heated up to T_{peak} and cooled back to T_0 = 0.36. Cooling was performed at the same rate as heating. Another 10^5 step period was run at T_0 = 0.36 after cooling and the resulting configurations was considered as the final structure. Our preliminary runs showed that

any T_{peak} < 0.82 was too low to cause any appreciable effect and the system remained with essentially the same initial order phase after cooling. On the other hand, any T_{peak} > 1.18 was too close to the boiling temperature and the thin film was no longer stable, resulting in most of the beads evaporating infilling the entire simulation box.

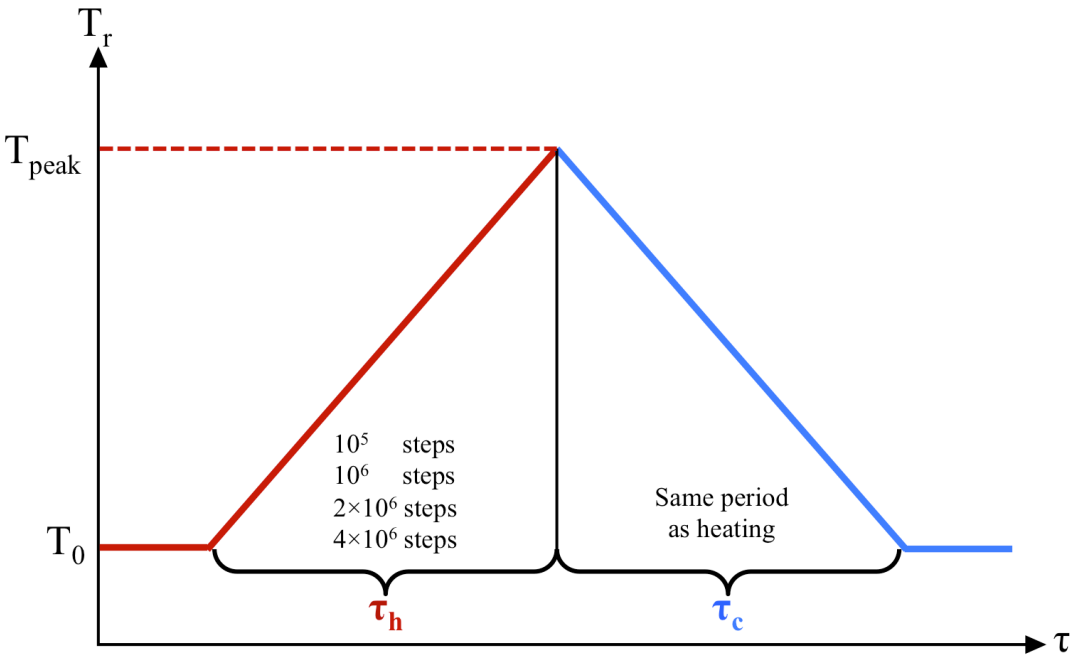

Figure 5. Schematic representation of the simulation procedure. System was heated up to peak temperature, T_{peak} with different heating ramp periods, τ_h and cooled with cooling ramp period, τ_c. The heating and cooling ramp periods are kept equal throughout the simulation cycle. A 10^5 steps run was performed before τ_h and after τ_c at T_0.

Different values of $\varepsilon_{substrate}$ were tested to study the preference of substrate. Since our model has linear chains with equal number of A beads and B beads, the equilibrium order phase should be a lamella phase. Also, the orientation of the ordered lamella structure will depend on the substrate selectivity.

2.1.2 BCPs Bulk Simulation

Step Heating

Bulk simulations were performed with an isothermal-isobaric (NPT) ensemble (to allow volume fluctuations) to predict the bulk phase behavior which can serve as reference. 1500 chains were contained in the simulation box imposing periodicity in all three dimensions. T_r was initially set at 0.43 and P* was maintained at 1 to preclude any evaporation from taking place. ε_{AA}, ε_{BB} and ε_{AB} were all initially set to 1.9 for a 5×10^4 steps run to create a fully mixed state and a disordered initial phase. After this initial period, ε_{AA}, ε_{BB} and ε_{AB} were set back to the "correct" thin film values (given in Table I) and run for 2×10^6 steps to allow phase segregation to take place. Pressure was ramped down from one to zero in all three directions during this 2×10^6 steps run to allow the system to attain its equilibrium dimensions. The simulation was then continued under zero pressure until lamella phase was formed.

The lamella phase obtained above was then used as an initial configuration to explore the bulk phase behavior at different temperature. Since lamella phase is an order structure with 2D domains of lamella, we allowed the pressure to vary independently along the parallel and perpendicular directions to the lamella plane [32]. Starting from $T_r = 0.43$, the temperature was raised by 0.036 and maintained for 2×10^6 time steps then the temperature was raised again until the system disordered. The box was elongated in the direction parallel to the lamella plane and the initial cubic shape gradually became a rectangular cuboid during the heating process.

Relaxation Time

To quantitatively compare the simulation heating/cooling ramp period to the experimental laser annealing cycle time scale, we calculated the relaxation time of our dBCP model from the response of the system to shear deformation. This relaxation time captures the linear viscoelastic behavior of the dBCP as the time required to respond to the applied stress to obtain the steady state. We thus performed these simulations under different shear rates, where the shear stresses developed parallel to the bulk lamella plane [48][49]. The relaxation time was determined from the reciprocal of the shear rate at which the viscosity decreases; i.e., at the onset of shear thinning. To allow for comparison to experimental data, the simulation temperature was maintained at $T_r = 0.93$ to match the temperature (419.15 K) at which relaxation experiments for polystyrene (weight-average molecular weight = 800,000) were conducted via photon-correlation spectroscopy [50], where the relaxation time can be measured at higher temperature (i.e., close to T_{ODT}) and the results agree well with simple shear stress relaxation experiment [51] (noting that the $T_{ODT} = 450.15$ K for the dBCP PS-b-PMMA used in laser annealing experiment [21]). The results provided in Table 2 show that our simulated heating/cooling ramp period is of the same order of magnitude as experimental laser annealing time scale. These results also help illustrate the idea that laser annealing times are long enough to allow chains to locally relax, but not too long to dwarf the (temperature-dependent) time scale of the order-disorder transition (otherwise any heating cycle with $T_{peak} > 1$ would invariably result in complete disordering of the lamellar phase).

Table 2. Comparison of relaxation and ramp times

	Experimental Results	Simulation Results
Relaxation time	80 μs [50]	312.5 τ
Heating/cooling period	0.25 ~ 10 ms [21]	500 ~ 20000 τ
$\frac{\text{Heating/cooling period}}{\text{Relaxation time}}$	3.125 ~ 125	1.6 ~ 64

2.2 Order Parameters

2.2.1 P2 Order Parameter

To characterize the global order of the thin film, we adopted the algorithm described by John *et al*. [33] based on the global order parameter $\langle\overline{P_2}\rangle$ to measure the order of the system, and $\overline{P_2}$ is defined as:

$$\overline{P_2} = \max_{n} \frac{1}{N_a}\sum_i \frac{1}{2}(3|\boldsymbol{u}_i \cdot \boldsymbol{n}|^2 - 1) = \max_{n} \frac{1}{N_a}\sum_i \frac{1}{2}(3\langle cos^2\theta_i\rangle - 1) \quad (4)$$

where, N_a is the number of chains, $\boldsymbol{u}_i$ = [$u_{i,x}$, $u_{i,y}$, $u_{i,z}$] is the unit vector along the end-to-end vector of chain i, and **n** = [n_x, n_y, n_z] is the director unit vector for which $\overline{P_2}$ is maximized. For a disordered system, the chains have no preferred alignment direction; P_2 approaches a value close to 0. Conversely, P_2 approaches 1 for an ordered system where all the chains lie parallel in a reference direction. If the orientation is perpendicular to the reference direction, the value of P_2 approaches -0.5 [34]. Based on our bulk simulation result, the end-to-end vectors tend to align normal to the lamella plane and the histogram showed a large P2 value of both end-to-end vectors and centroid of blocks vectors, as illustrated in Figure 6.

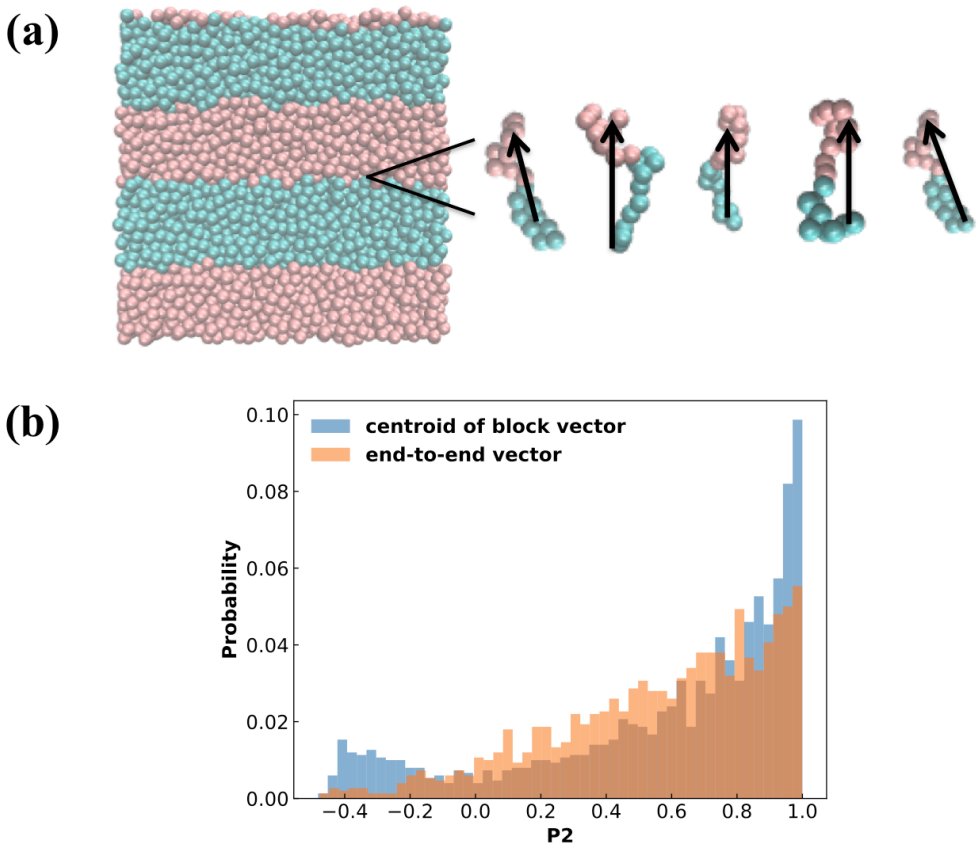

Figure 6. Schematic representation of the bulk lamella phase. (a) Snapshot representing end-to-end vectors of dBCP chain showing that the vectors point normal to the lamella interface plane (b) Histogram of P2 value of centroid of block vectors and end-to-end vectors showing that the trends are similar.

2.2.2 Average Alignment of End-to-End Vectors

While P2 can provide an insight of how well the system is ordered, it can't tell the quantitative difference between two systems with similar ordered structure but with chains oriented in different direction with respect to the substrate. Capturing such difference is crucial for systems undergoing a heating program that disorders the phase since then upon cooling the ordered state will be re-established but with potentially different features. To quantitatively examine the orientation of the system, we adopted

an order parameter ∅ [26] defined as:

$$\emptyset = \frac{1}{N}\sum_{i}^{N}|\boldsymbol{u_i}\cdot\boldsymbol{n}| \quad (5)$$

where N is the number of chains, $\boldsymbol{u}_i$ is the unit end-to-end vector and $\hat{n}$ is the reference vector.

∅ measures how well the molecules align along the reference direction. Considering the lamella alignment for different types of substrate, the reference vector was chosen to be the maximum lamella alignment direction calculated from the recipe described by John *et al*. [33] for systems with vertical lamella, and the z-direction (normal to the substrate) for systems with horizontal lamella.

If the ordered direction is aligned parallel to $\hat{n}$, ∅ will approach a value close to 1. If the system is aligned perpendicular to $\hat{n}$, ∅ will close to 0. As a result, for both ∅ close to 1 or 0, the system is ordered. For ∅ close to 0.5, the system is typically disordered since it would indicate no preferential alignment. We can track the evolution of ∅ to see whether the system becomes fully disordered during heating. If the system maintains the initial order, then ∅ will have a value close to 1. If the system becomes fully disordered, the final structure will be independent to the initial configuration and the ∅ value will show a distinctive drop to values close to 0.5.

A local ∅ can also be used to quantify the ordering mechanism of the thin film at varying distance from the substrate, to examine the effect of the substrate and the free surface. For this we divided the thin film into four equal thickness layers in the z direction: bottom (layer 1), layer 2, layer 3 and surface (layer 4), and calculated ∅ for

each layer during each time step to examine the effect of heating and cooling on the ordering profile.

2.2.3 2D Structure Factor

Structure factor is calculated based on Eq. (6) [35] to detect the translation order in the system,

$$S(\vec{q}) = \frac{(\sum_j \cos(\vec{q} \cdot \overrightarrow{r_j}))^2 + (\sum_j \sin(\vec{q} \cdot \overrightarrow{r_j}))^2}{N} \quad (6)$$

where **q** is the wave vector, the $\mathbf{r}_j$'s are the position vectors of each beads, and N is the number of beads.

The wave vector **q** is restricted to integer numbers of wavelengths within the simulation box, namely, $\vec{q} = 2\pi(\frac{n_x}{L_x}, \frac{n_y}{L_y})$ and the peak location is given by $m = \sqrt{n_x^2 + n_y^2}$, which is unique to different space group symmetries. For lamella phase, the locations of peaks have the following ratios (1:2:3:4:5...). To better visualize S(q) and give a comparison to experimental GIWAXS results [18], we ignore the thickness z and consider our thin film system as a pseudo 2D structure and plot the S(q) based on the position of q_x and q_y. This 2D S(q) plot can provide details of the structure in the system as well as the direction of the spatial alignment in the ordered lamella phase.

2.2.4 Roughness Parameter

To quantitatively capture the extent of surface roughness of the island phase, we defined an order parameter "*RP*". We discretize the xy plane into a 50×50 grid to produce $N = 2500$ square tiles and calculated the polymer height of each tile H. The order parameter RP is defined as the ratio of the standard deviation of the height of the tiles and the thickness of the initial horizontal (flat) lamella phase H_0:

$$RP = \frac{\sqrt{\langle H^2 \rangle - \langle H \rangle^2}}{H_0} \quad (7)$$

If the phase is close to have fully horizontal lamella layers, the surface will be nearly flat and smooth and RP approaches a value close to 0. As the island phase forms, the surface roughness will increase and so will the value of RP.

2.2.5 Surface Area Parameter

The coordinates of the xy plane grids obtained from 2.2.4 are further used to estimate the surface area of the island phase by a triangulating that uses the tile centers as triangle vertices (i.e., two triangular areas are defined by four neighbor grids, as illustrated in Figure 7). The area of each triangle was found from the cross product of the vectors forming two edges of a triangle. Note that the calculation of surface area will depend on how finely discretized is the grid to mesh surface; however the relative trends of surface area changes with annealing conditions will be similar. Thus, the relative surface area parameter SP is defined as the ratio of the surface area of the island phase and the initial horizontal lamella phase:

$$SP = \frac{\text{Surface area of island phase}}{\text{Surface area of initial horizontal laemlla phase}} \quad (8)$$

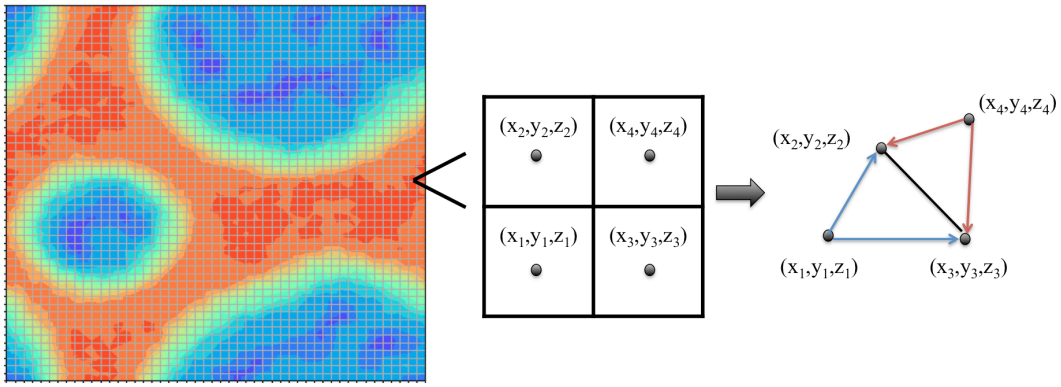

Figure 7. Schematic representation of surface area calculation. The surface area is computed by the triangulating over the preset grid points and adding the area of each triangle (found as half the norm of the cross product of neighbor grid vectors).

CHAPTER 3

RESULTS AND DISCUSSION

3.1 Bulk Phase Behavior

To understand the dBCP lamella phase behavior, we simulated a bulk system to see the way a lamella phase disorders upon heating in the absence of external interfaces, as shown in Figure 8. For these simulations the system was fully equilibrated at the different temperatures and hence could be seen as corresponding to an infinitely slow heating rate.

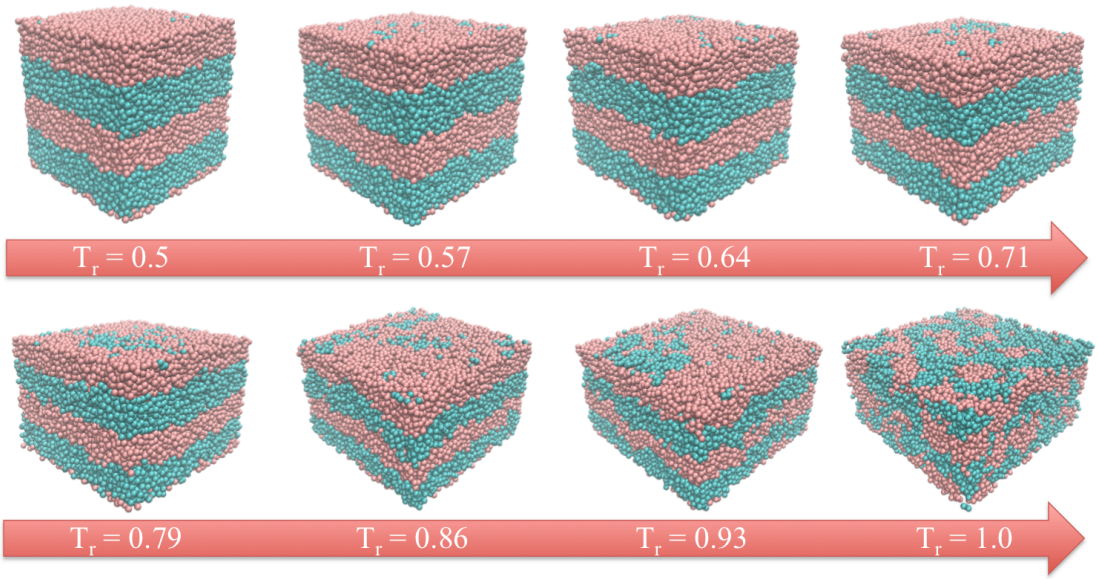

Figure 8. Snapshots of bulk phase behavior at different temperatures.

The bulk phase experienced a stretching parallel to the lamella plane as temperature increased until the phase disordered. The lamella spacing and end-to-end distance both decreased. The order-disorder transition occurred approximately at T* = 2.8 (in reduced LJ units) which henceforth corresponds to T_r = 1, above which the blocks fully mixed and the lamella phase no longer existed. Also, the area of the xy plane (parallel to lamella phase) increased with temperature, which implies a decrease of the bead surface density per layer (i.e., bead number per area per layer), a result of the decreasing segregation strength between blocks (i.e., χN), as shown in Figure 9.

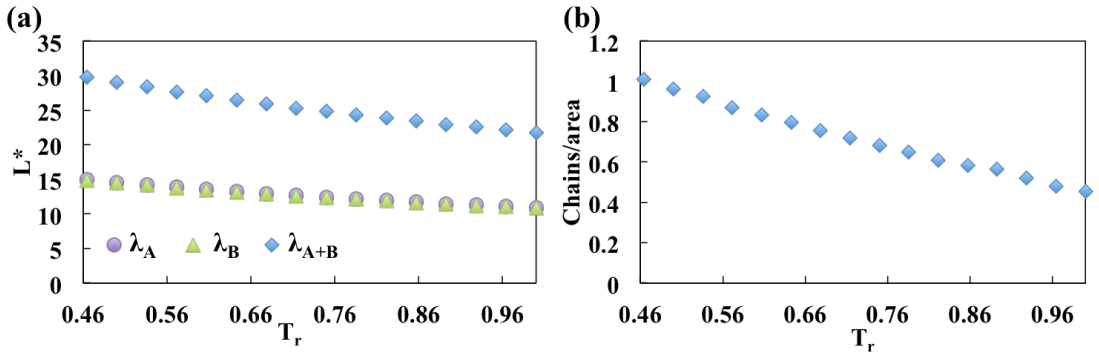

Figure 9. Bulk simulation results of (a) Lamella spacing (λ) as a function of T_r (b) Chain number per unit area on xy plane per layer as a function of T_r.

3.2 Ordering Mechanism of BCPs Thin Film

3.2.1 Effect of Substrate Selection

In the following sections, we studied the dBCP thin film under a soft confinement to examine the effect of the solid substrate and free interface. The ordering mechanism

for both neutral and selective substrate can be captured by tracking ∅ at each time step. Figure 10 shows the case of 3000 chains as illustration.

With a neutral substrate, the ordered lamella structure is perpendicular to the substrate (i.e., a vertical lamella phase) and the ordering process occurred simultaneously through all layers and reached a similar final value of ∅, as shown in Figure 10 (a). In contrast, for the B bead selective substrate, the ordering process leads to a lamella phase parallel to the substrate (horizontal lamella phase). The bottom layer was rapidly populated by the favored B beads as they attached parallel to the substrate, leading to a rapid increase of ∅ (0.4 → 0.7) during the initial 10^6 steps. The ordering process then propagated to the upper layers. As the distance to substrate increased (from layer 2 to the surface), the polymer chains were aligned more perpendicular to the substrate to form the favored horizontal lamella phase, resulting in increasing values of ∅, as shown in Figure 10 (b).

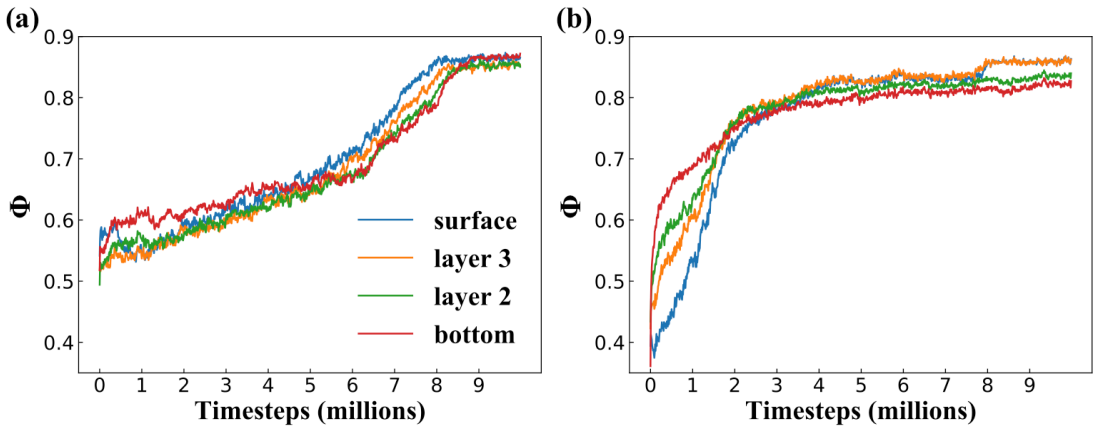

Figure 10. Order parameter history for 3000 chains system obtained at T_r = 0.54 with (a) neutral and (b) selective substrate favoring B beads.

3.2.2 Effect of Surface Tension

Surface tension plays an important role in the ordering of the system with a selective substrate. For varying number of chains in the system, the total height of the dBCP layer changes and by having a selective substrate favoring A or B beads, the lamella period and orientation will have different arrangements, as shown in Figure 11.

When the surface layer tends to be populated by the higher surface tension beads (i.e., those with a higher self-attraction ε which are the A beads in our system), a horizontal arrangement is unfavorable and the system will tend to form a vertical lamella, which allows some of the lower surface tension beads to come up to the free surface. When the lower surface tension beads tend to populate the surface layer, the horizontal lamella phase is formed.

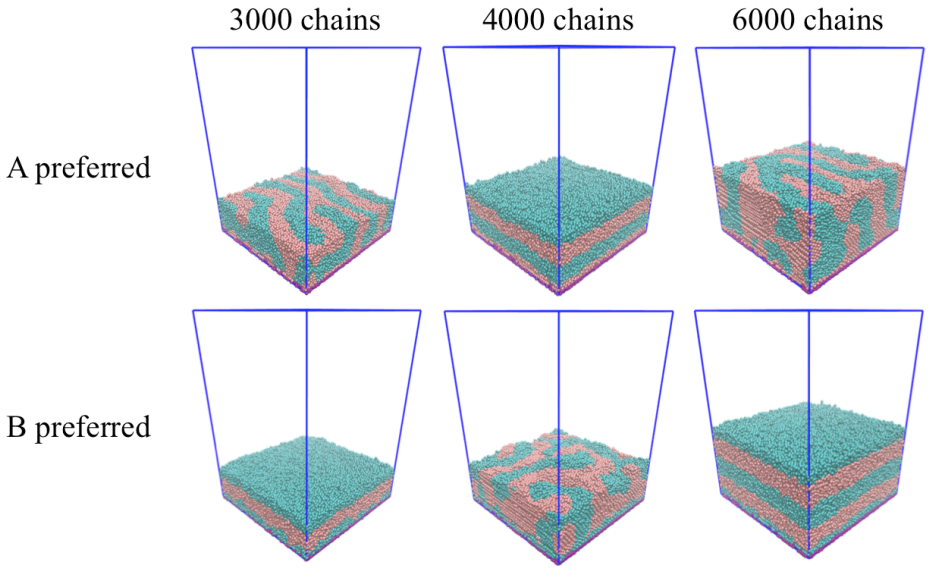

Figure 11. Snapshots of systems with varying number of chains and different selective substrates at $T_r = 0.54$, showing the effect of surface tension and lamella period on the morphology.

3.3 Heating/Cooling for Different Ramp Periods on Neutral Substrate

3.3.1 3000 Chains System

Fast Heating and Cooling

The thin film response for each layer (bottom → surface) to temperature changes can be observed by tracking ∅. Figure 12 shows this results for the case of fast heating/cooling ramp period (10^5 steps) at different T_{peak} (from 0.82 to 1.18).

At low T_{peak} (= 0.82), only the surface layer was affected on heating as indicated by a small drop in the ∅ value (0.85 → 0.75) during heating while the remaining layers (bottom, layer 2 and layer 3) stayed ordered with an average ∅ value greater than 0.85 over the entire heating and cooling periods. The entire system was able to go back to initial ordered state after cooling. Figure 12 (a) shows a snapshot and the 2D structure factor color map of the final ordered phase after the heating and cooling cycle; in the bottom panel it also shows the variation of ∅ value for each layer during the heating and cooling process for T_{peak} =0.82. As T_{peak} increased ($1 \leq T_{peak} \leq 1.14$), a large drop in ∅ value was observed due to the disordering of layers 2, 3 and surface layer during heating, while the bottom layer was able to sustain more of the initial order, as show in Figure 12 (b). The final structure obtained in this temperature range was similar as the initial lamella phase with some defects in lamella spacing, as detected in the 2D structure factor color map by the diffuse parallel peaks. If T_{peak} is even higher (= 1.18), the system fully disorders and the final structure stays disordered due to the short cooling period, as shown in the snapshot and the ring shape 2D structure factor (Figure 12 (c)).

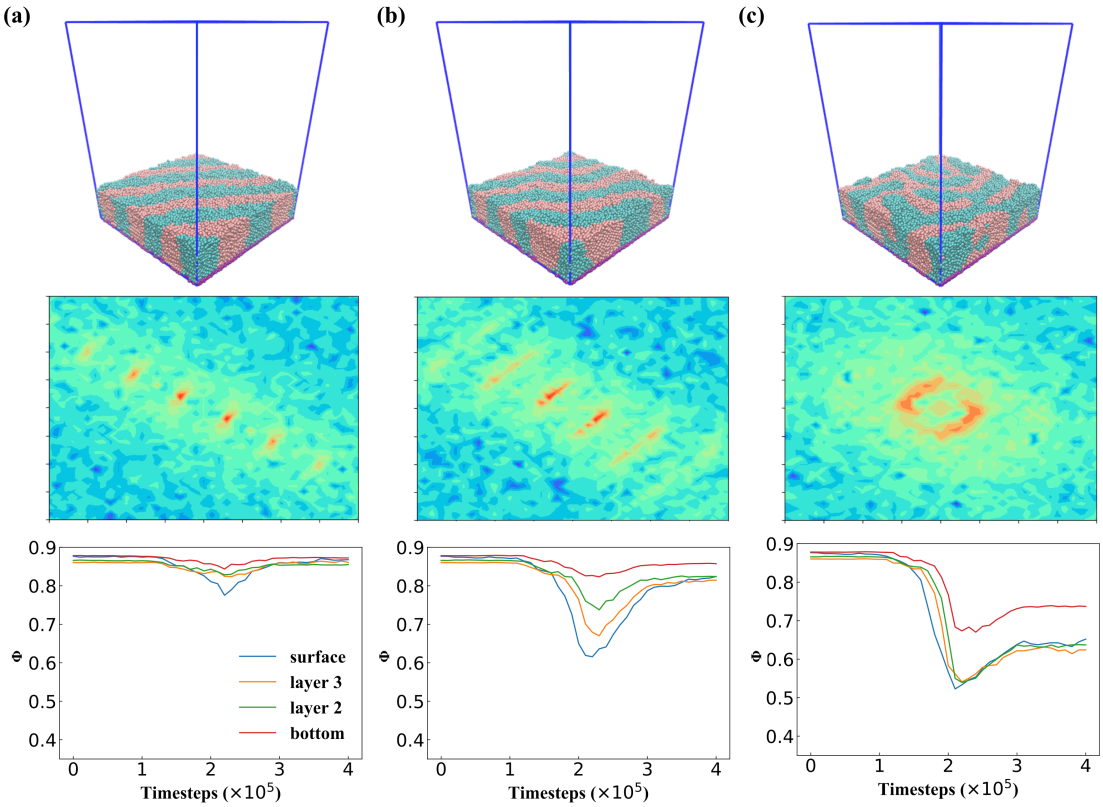

Figure 12. Snapshot, 2D structure factor of final structure at T_0 and Ø history for 10^5 step heating/cooling for three peak heating temperatures: (a) 0.82, (b) 1, and (c) 1.18.

Slow Heating and Cooling

For 10^6 steps heating/cooling ramp period, the system's structure was affected not only in the surface layer but also layers 2 and 3 even at the low T_{peak} = 0.82 because of the larger amount of heat (energy) dumped into the system during the longer heating period. For T_{peak} = 1.0, a similar trend was observed as with T_{peak} = 0.82 but with all the layers showing a larger decrease in the Ø values while heating, indicative of higher disorder in the respective layers. After cooling, the system ordered back to the initial lamella phase. Note that the system is disordered at T_{peak} = 1.14, a temperature lower

than that at which disorder ensued with fast heating (10^5 steps ramp period) because the system got longer time to absorb thermal energy, as shown in Figure 13.

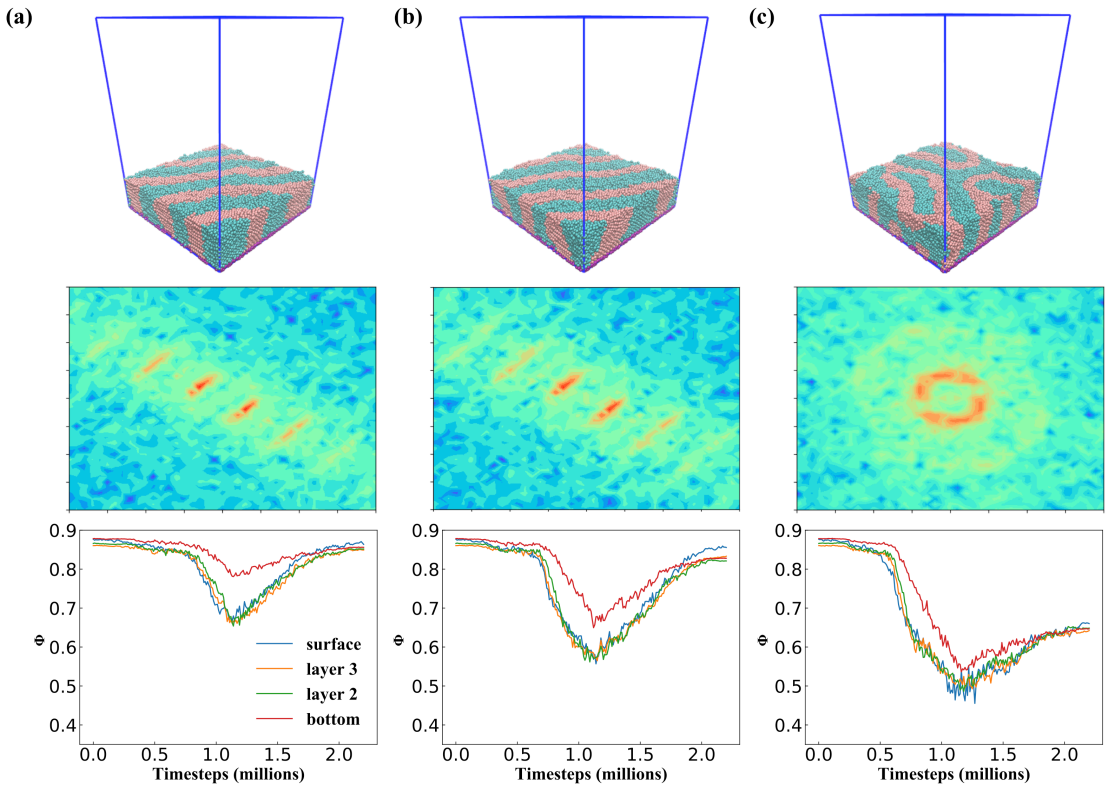

Figure 13. Snapshot, 2D structure factor of final structure at T_0 and Ø history for 10^6 step heating/cooling for three peak heating temperatures: (a) 0.82, (b) 1, and (c) 1.14.

Relationship Between Peak Heating Temperatures and Heating/Cooling Periods

In this section, we evaluate the apparent T'_{ODT} at different heating and cooling ramp periods using P2 and Ø order parameters to compare with the experimental results reported by Jacobs *et al* [21].

To quantitatively examine the disorder peak temperatures at different heating/cooling ramp periods, P2 values were calculated for the final structure after

the heating/cooling cycle as shown in Figure 14. As the heating ramp period gets longer, the order-disorder transition temperature decreases and approaches the bulk T_{ODT}. For the longest heating and cooling ramp period (4×10^6 steps), the T'_{ODT} occurs between T_r = 0.93-0.96, with a P2 dropping from 0.6 to 0.53 while forming a final partially ordered structure.

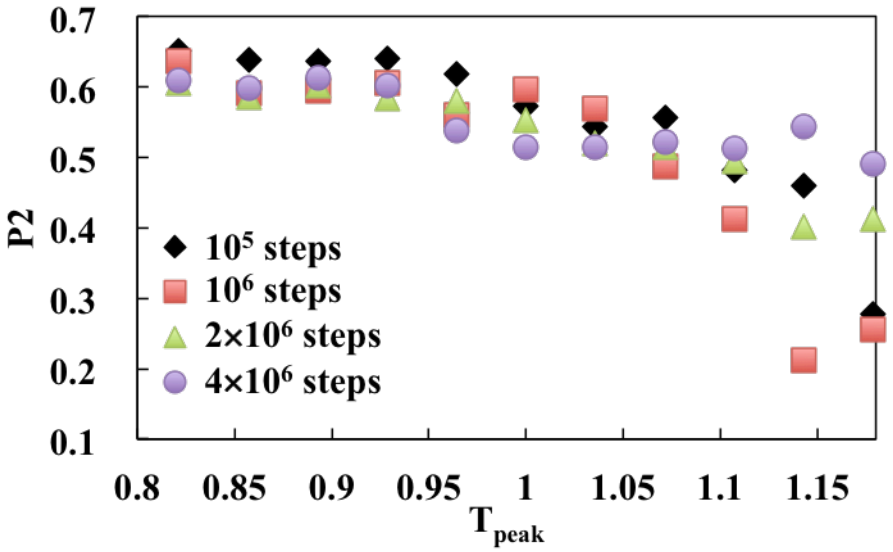

Figure 14. P2 of the final structure at T_0 after different heating/cooling ramp periods as a function of peak heating temperature. System has 3000 chains.

By combining the results of P2 and ∅ (see Figure S1 and S2 in the appendix), we can detect the temperature where the system is partially and completely disordered, these results are compiled in Figure 15. The relationship between disordering temperature and heating/cooling ramp period obtained with our simulation model is consistent with the experimental results, showing that faster heating and cooling rate disordered the system at a higher T_{peak}.

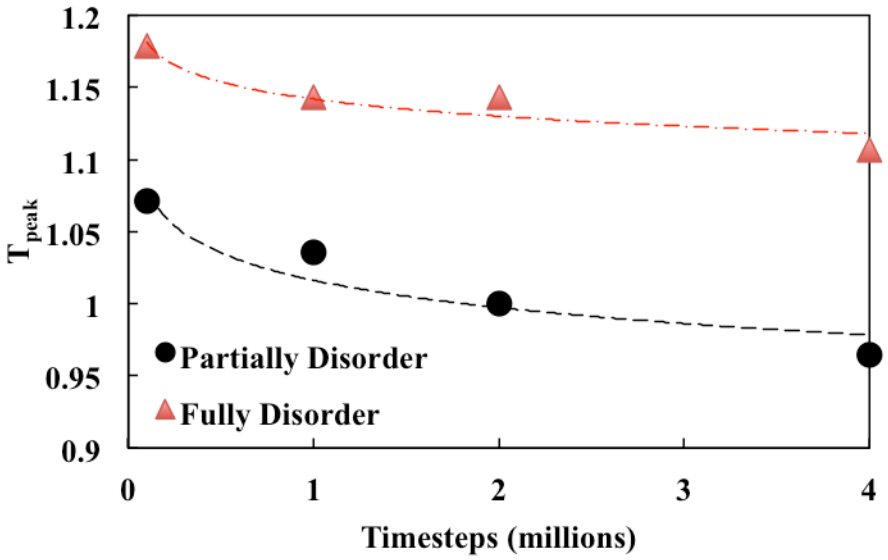

Figure 15. Heating temperature where the system started to disorder and where became fully disordered (T'_{ODT}). Shorter heating/cooling ramp period corresponds to a higher disordering temperature.

The order-disorder transition is related to the energy gained by the system during the heating cycle. Figure 16 shows the total system energy at each T_{peak} that is above T_{ODT} for different heating/cooling ramp periods. For the slowest heating cycle (4×10^6 steps), the system was fully disordered at $T_r = 1.11$ with a total system energy value of 2.3148, corresponding to a energy level that is required to disorder this system. The shorter ramp periods have to go to a higher T_{peak} to achieve such energy level, which results in a higher T'_{ODT}.

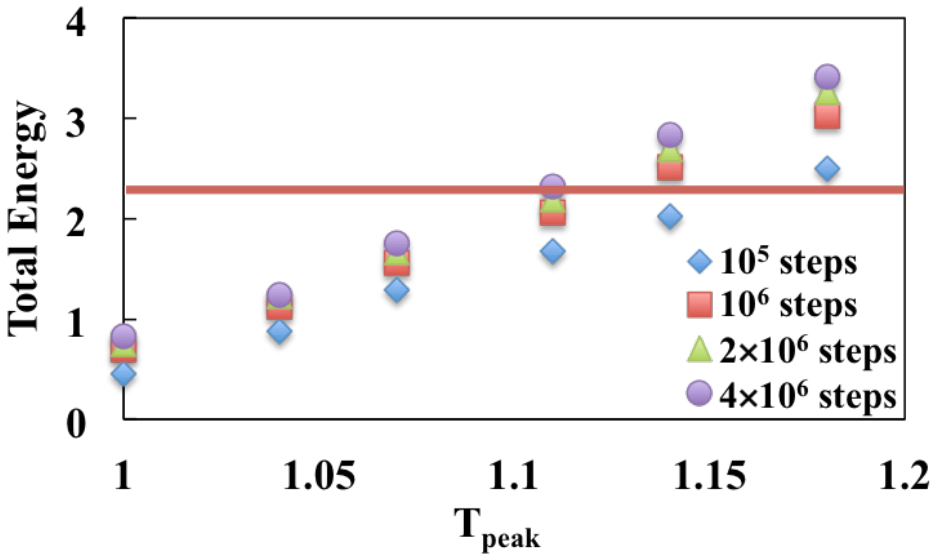

Figure 16 Total system energy (in units of ε) at each T_{peak} under different ramp periods. Red line denotes the lowest disordering energy in our simulation.

3.3.2 4000 and 6000 Chains System

The effect of film thickness is also examined by using systems with 4000 and 6000 chains while keeping the substrate area constant. The P2 results for these systems are shown in Figure 17.

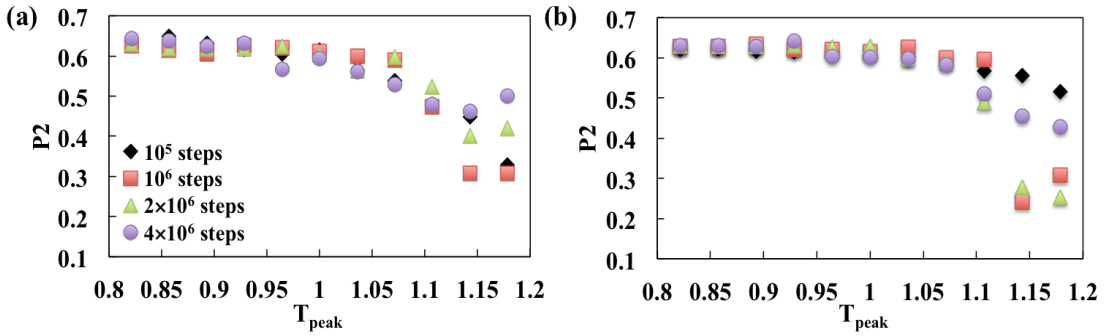

Figure 17. P2 of the final structure at T_0 after different heating/cooling ramp periods as a function of peak heating temperature for (a) 4000 and (b) 6000 chain system.

The 4000 chain system exhibited a similar order-disorder transition trend as that with the 3000 chain system. The 6000 chain system showed more stability during the heating cycle, leading to a higher T'_{ODT} even for longer heating/cooling ramp period. This clearly illustrates the inverse relation between film thickness and T'_{ODT}, which is consistent with the experimental findings of Kim *et al.* [46]. The effect of thickness and heating/cooling ramp period can also be extracted by using Ø for different layers. For 10^5 steps heating/cooling, the substrate attraction can hold the bottom layer to sustain this rapid temperature variation to largely retain the initial order, so that the disorder transition happened mostly on the surface. The 3000 and 4000 chain systems showed a tendency to disorder from surface to layer 2 for $T_{peak} > 1.14$ and only the bottom layer was able to remain partially ordered relative to the initial state. For the 6000 chain system, the initial ordered structure can be sustained even for $T_{peak} = 1.18$ as shown in Figure 18.

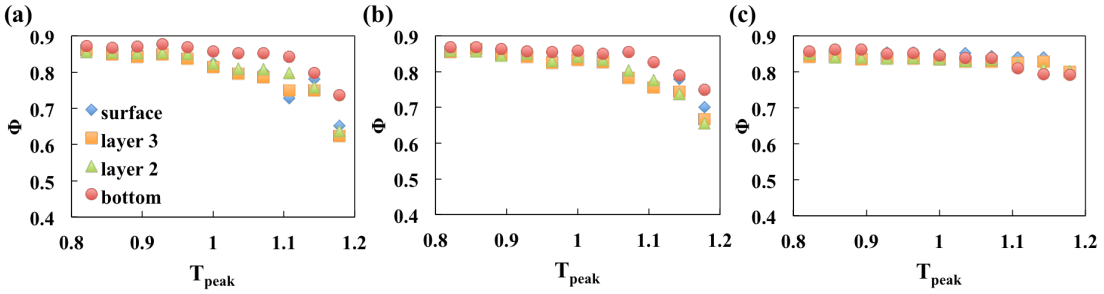

Figure 18. Ø of the final structure at T_0 after 10^5 step heating/cooling ramp period as a function of T_{peak} for systems with (a) 3000, (b) 4000, and (c) 6000 chains.

On the other hand, for heating/cooling ramp period longer than 10^6 steps, all three systems showed a disorder transition through the whole thin film. Also, the disorder happened at lower temperature for thinner films, as shown in Figure 19.

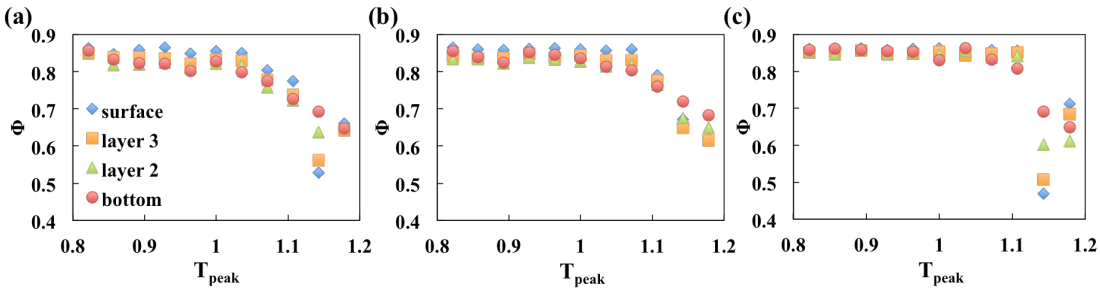

Figure 19. Ø of the final structure at T_0 after 10^6 step heating/cooling ramp period as a function of peak heating temperature for systems with: (a) 3000, (b) 4000, and (c) 6000 chains.

3.4 Heating/Cooling under Different Ramp Periods on Selective Substrate

3.4.1 10^5 Steps Heating/Cooling

For 10^5 steps heating/cooling, the horizontal lamella phase remained largely unperturbed at the bottom layers, indicating that the substrate attraction was strong enough to effectively anchor the selective domain segments. The range of the substrate attraction does not reach the top layers and so the chains in those layers tended to expand to the free surface at high temperatures. This disordered surface structure created during heating did not recover a state of order after the rapid cooling, as shown in Figure 20.

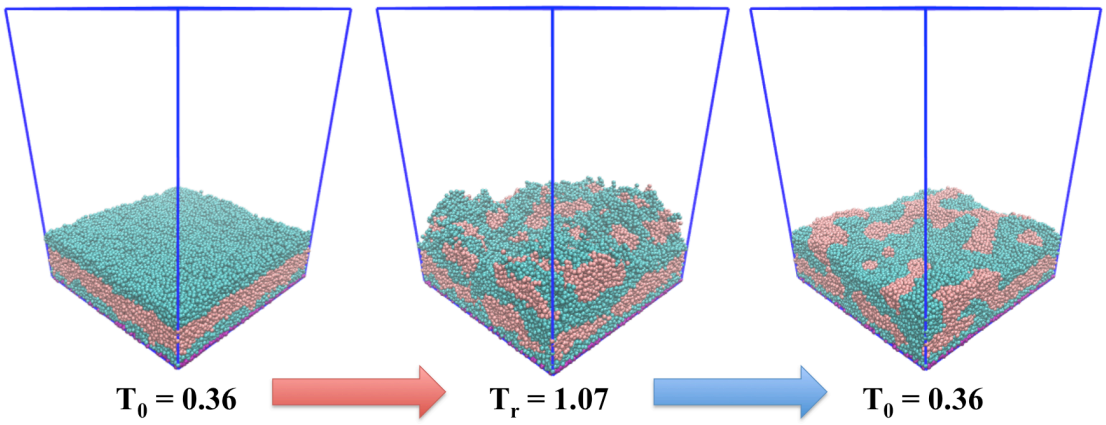

Figure 20. Illustration of the structural changes after heating and cooling a fully horizontal lamella phase with 10^5 steps per ramp.

3.4.2 Formation of Island Phase

On the other hand, when using 10^6 and 2×10^6 steps heating/cooling the system formed an interesting "island" phase after cooling. This imperfect horizontal lamella layers were obtained whether we started from a system with initial order state or a disorder state, and whether A or B favored substrate. Forrey *et al.* [26] has provided an explanation for the island phase formation while heating a dBCP film from an initially disorder phase. The energetic (substrate) interactions that favors the fully horizontal lamella phase competes with the entropic effects that favor chain stretching and disorder; the islands formed when the free energy penalty of chain stretching is more dominant. However, here we find that the island could also be obtained during a heating and cooling process even if the system already formed a fully horizontal lamella phase at T_{peak}. The lamella layer retreated to form island phase during cooling, as shown in Figure 21.

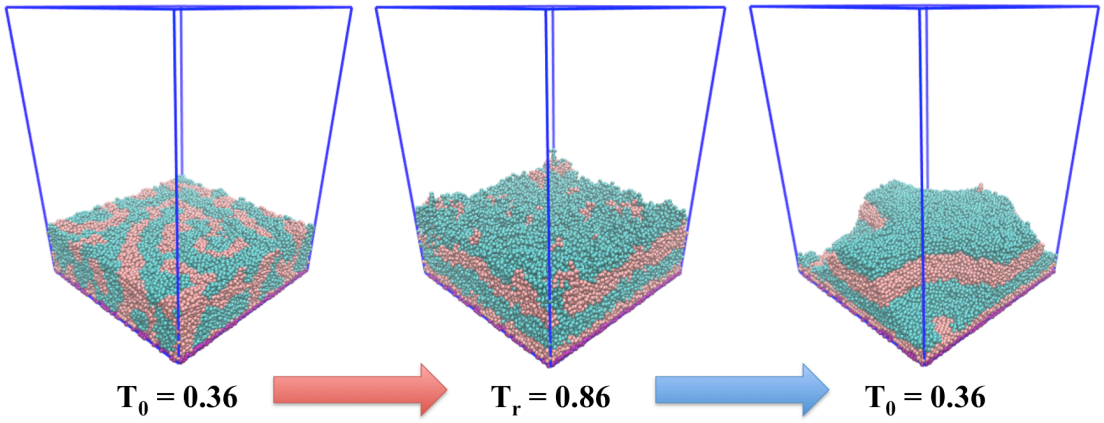

Figure 21. Illustration of an island phase formed after cooling from a fully horizontal lamella phase with 10^6 steps per ramp.

To understand the mechanism of island formation, we revisit the bulk phase behavior reported earlier in section 3.1. The tendency of lamella thinning and lower chain area density with temperature shown in Figure 9 can provide an explanation for the island formation. As the initial disordered phase is heated to a high temperature, the system tends to form fully horizontal lamella phase with thin layers at that temperature. As the temperature decreased as cooling started, χN increased and the attraction between like blocks also increased. As the system begins to favor thicker lamella (containing more chains in each layer), the system reached a structural instability that tends to rearrange the formerly formed horizontal lamella phase, causing some layers to retreat or partially disappear. The surface islands can then be seen as resulting from the freer surface layer being only partially incorporated into a deeper layer.

The island phase may also be formed from an initial ordered phase, as shown in Figure 22. As temperature increased, the chain density per layer per unit area

decreased. The initial lamella phase (and layer spacing) destabilized as χN decreased; hence some chains were "squeezed out" to form a new layer on the top. During cooling, these expelled chains were not able to penetrate back into the original layers due to a large free energy barrier associated with chains crossing unfavorable block domains. Thus, these chains remained kinetically trapped on the top and became part of the islands; indeed a clear evidence that the metastability of the island phase is the fact that they have larger potential energy than the equilibrium horizontal lamella phase at same temperature condition (T_0 = 0.36), as illustrated in Figure 23 (see also Figure S3 in the appendix for the reheating test showing that the island phase is hard to eliminate). Note also that the area of these islands shrunk after cooling, an observation consistent with the experimental results of Croll *et al.* [47]

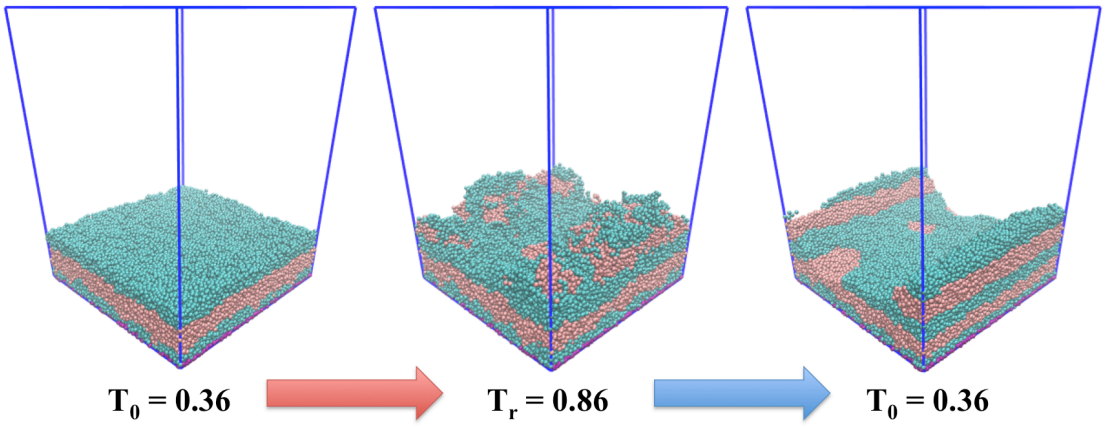

Figure 22. Illustration of island phase formed from an initial horizontal lamella phase.

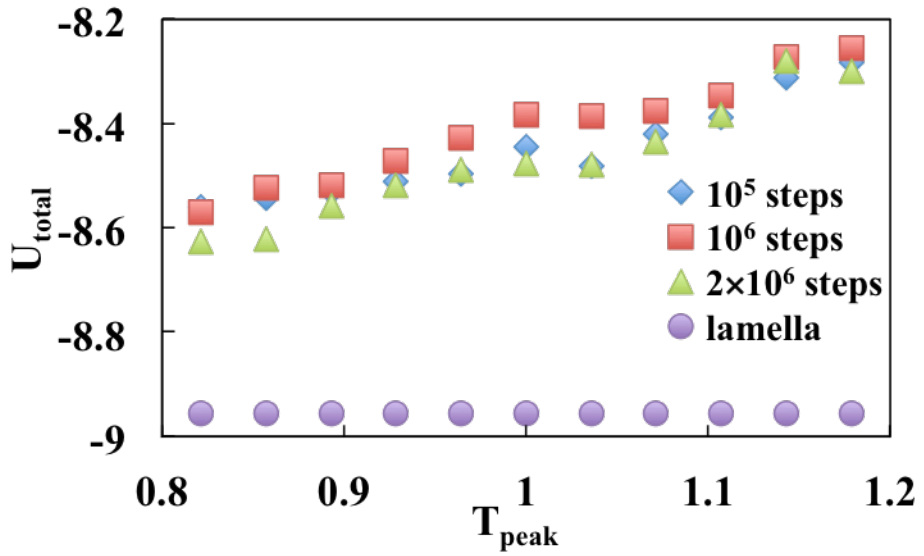

Figure 23. System potential energy (U_{total}) of the final structure at T_0 after different heating/cooling ramp periods as a function of T_{peak}. The U_{total} of the horizontal lamella phase at $T_0 = 0.36$ is shown for comparison. The system has 3000 chains.

3.4.3 Quantifying the Roughness of Island Phase

The rough topography of island phase and the concomitant increase of surface area could be exploited for applications where nanoscale features are desirable as in creating super-hydrophobic surfaces (via a mechanism akin to the lotus leaf effect) or enhance another type of surface activity. Our calculations of *RP* for the island phase showed that the roughness depends on both T_{peak} and τ_h/τ_c. Likewise, our results for the surface metric *SP* show that the surface area increases with heating temperature, as shown in Figure 24. Expectedly, the trends of RP are similar to those of SP as both metrics are correlated.

A higher T_{peak} leads to the formation of more horizontal lamella layers as the layers get thinner. These extra layers will partially remain as islands after cooling and cause the roughness to increase but only up to a point (i.e., increases taper to a plateau

value, see Figure S4.) A longer cooling period provides more time for the chains to rearrange to try to locally reach the optimal lamella spacing (driven by a larger χN), which resulted in the formation of islands at a lower temperature (i.e., for the initial disordered system at T_{peak} = 0.86-0.96, see Figure 24 (a)) and more variation in height (i.e., RP ~ 60 for 2×10^6 steps τ_h/τ_c, see Figure S5 (a) compared to RP ~ 50 for 10^6 steps τ_h/τ_c, see Figure S5 (b)).

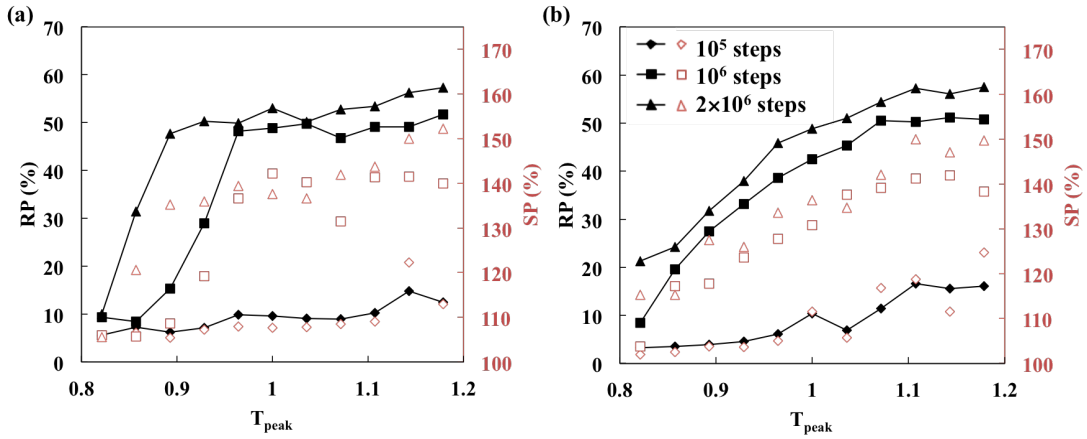

Figure 24. Roughness parameter (filled symbols) and surface area parameter (open symbols) of the island phase at T_0 for a system initially disordered (a) and ordered (b), as a function of peak heating temperature for 3 heating/cooling ramp periods.

To examine the effect of system's lateral size on island formation, we replicated the system four times and conducted the simulation under same conditions; representative snapshots are shown in Figure 25. This large system showed a more complex island phase contour and larger islands, indicating that there exists a finite size effect on roughness topography. However, the same general trend is observed of

roughness increasing with T_{peak} and with longer ramp period, as well as surface area increasing with T_{peak} (see Figure 26).

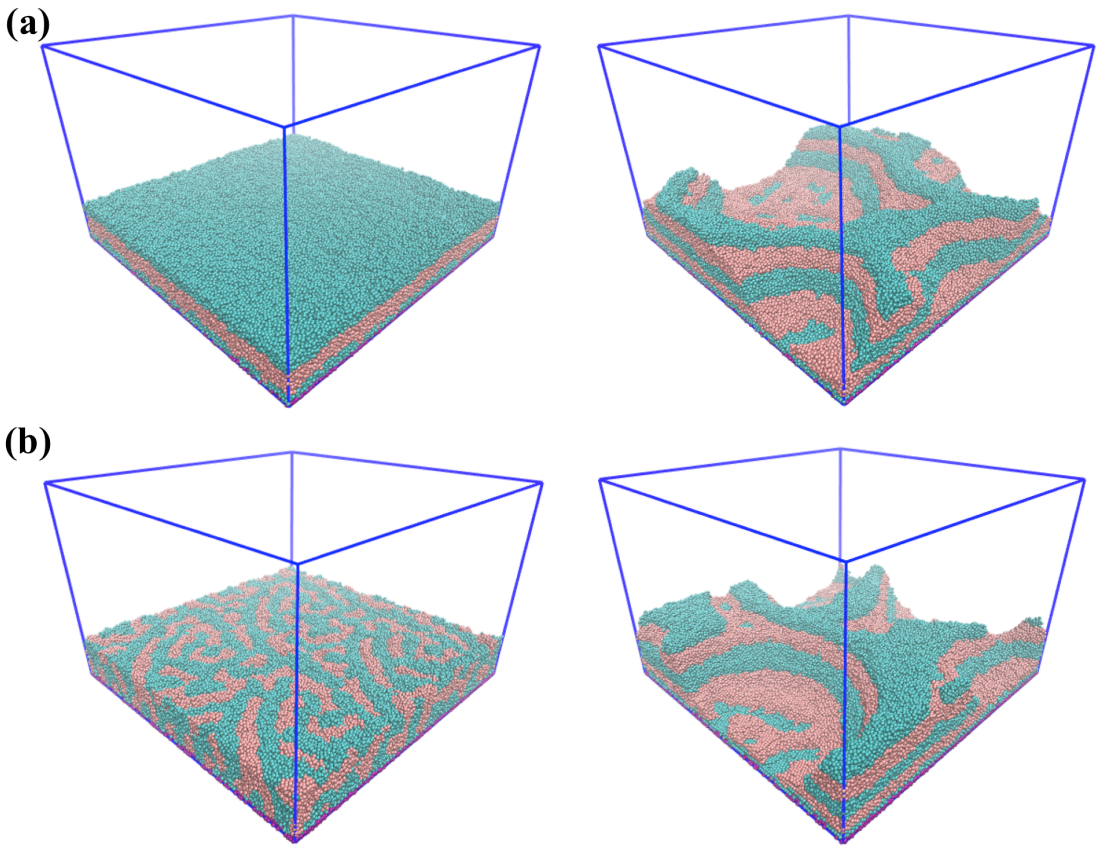

Figure 25. Sample results for system with larger surface area. Initially ordered (a) and disordered (b) configurations and the resulting island phases.

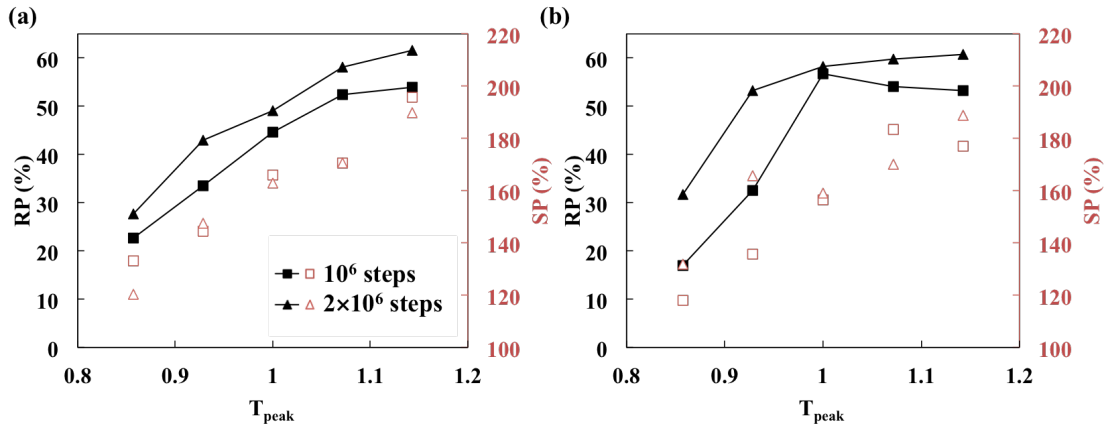

Figure 26. Roughness parameter (filled symbols) and surface area parameter (open symbols) of the initially (a) disordered and (b) ordered large system at T_0 as a function of peak heating temperature.

3.4.4 Formation of Hybrid Phase with 6000 Chain System

By using a larger system size while keeping the substrate area fixed, the overall thickness of the film is increased, which can give rise to more complex phases. Indeed for an initially disordered 6000 chain system, a hybrid structure formed having both horizontal and vertical lamella layers after the heating/cooling cycle. Note, however, that this system forms a fully horizontal lamella phase after annealing at T* = 1.5 for $5x10^6$ steps. A comparison of the hybrid phase and horizontal lamella phase is shown in Figure 27. The hybrid phase shows the effect of the local arrangements favored by both substrate and free surface simultaneously. The strong attraction to the substrate induces the formation of a horizontal lamella by the bottom layers as before. As temperature increased during heating, the upper layers tended to expand to the free volume above and being far from the substrate, the tendency for horizontal alignment diminishes. As a result, the upper layers arranged vertically next to the free surface in similar way as they would next to a neutral substrate.

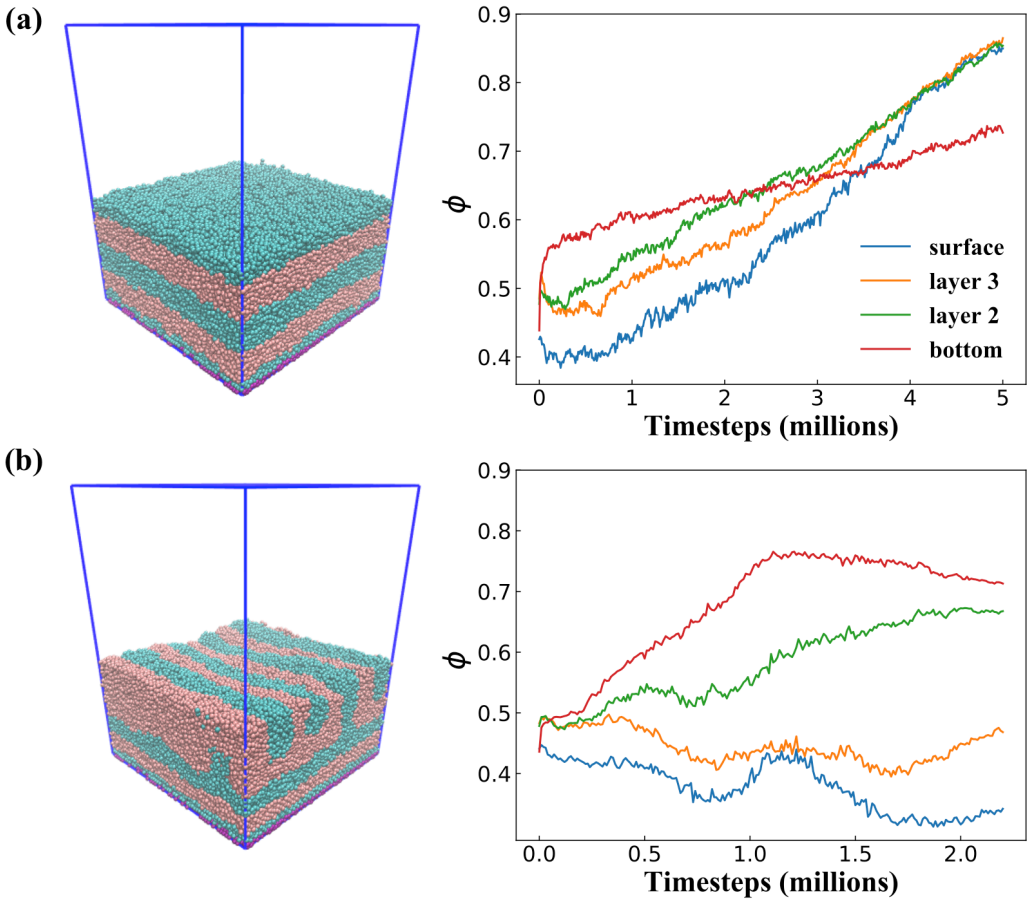

Figure 27. Snapshot and Ø parameter as a function of time step for (a) Perfect horizontal lamella phase formed at T_r = 0.54, and (b) Hybrid phase formed after heating/cooling at T_{peak} = 0.93 at 10^6 steps ramp period.

The orientation of the lamella phase can also be changed for thicker films with different heating/cooling cycles as illustrated for the 6000 chain system in Figure 28.

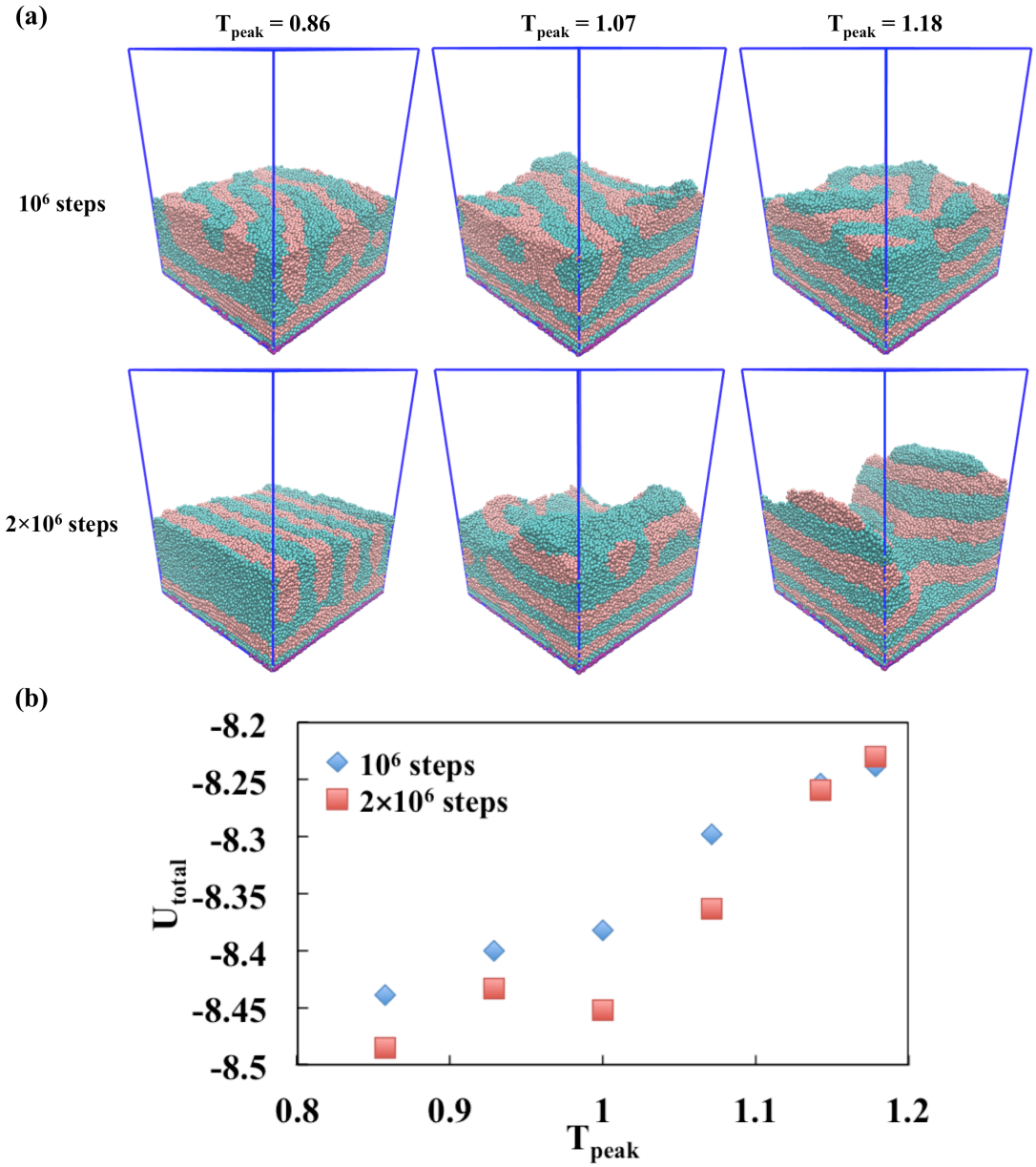

Figure 28. (a) Morphology of the 6000 chain system and (b) system potential energy at T_0 after heating/cooling cycle, showing the effect of peak heating temperature and heating/cooling ramp period on the lamella orientation of the final structure.

With a higher T_{peak}, the surface layer will gain sufficient freedom to arrange in a way to favor the lower surface-tension beads to come on top forming an extra horizontal layer. Along with a longer heating/cooling ramp period, the system has

more time to rearrange and form the island phase, absorbing the large energy dumped into the system during the heating cycle. Thus, the horizontal lamella alignment could be formed (albeit giving rise to the island phase) with higher T_{peak} and slower heating and cooling rate, as illustrated with the result for 2×10^6 steps heating/cooling and T_{peak} = 1.18. Note however, that the mixed horizontal/vertical lamella morphology like the one shown in Figure 28(a) would likely be the most thermodynamically stable phase at at T_0 given that it has the lowest potential energy (as shown in Figure 28(b)) compared to the other morphologies.

CHAPTER 4

CONCLUSION

Motivated by recent findings from an experimental laser annealing study [21], our simulation work investigated the dBCP thin film morphology under different heating cycles and substrate conditions using a simple coarse-grained model [26]. In particular, we explored the lamella phase behavior with respect to changes in peak temperature and heating/cooling ramp period. Our simulations results capture a similar trend for the order-disorder transition as in experiments, where faster heating/cooling rate leads to an increase of the disordering temperature for the vertical lamella phase formed on neutral substrates.

Simulations with a selective substrate revealed the formation of a long-lived metastable phase having horizontal but incomplete layers that give rise to a rough surface topography. This island phase formed after relatively long heating/cooling ramp cycles, and was independent of the initial structure (ordered or disordered) and substrate selectivity for either block. The nanoscale roughness features of this island phase which could be of potential use to modulate the wettability of surfaces. We found that the degree of roughness can be controlled to some extent with suitable choices of the heating temperature and heating/cooling rate.

For bulk and thin layer systems, a general trend observed in the lamella phase is that the lamella thickness decreases (and the chain surface density hence decreases) with temperature, which can result in the formation of new (potentially incomplete)

lamella layers. This domain thinning phenomenon can be seen as a stage preceding domain disintegration and mixing that occurs above the order-disorder temperature for all systems (bulk and thin-films with vertical or horizontal lamella). In a thin-film favoring horizontal lamella where additional surface layers formed during heating, the subsequent cooling increases the block segregation strength (χN), which thermodynamically promotes the consolidation of layers but kinetically promotes the trapping of some of the outer layers in a in partially filled states. The latter gives rise to the island phase which was found to be hard to eliminate once formed, i.e., reheating the islands led to final states showing a consistent degree of roughness.

A hybrid phase having both vertical and horizontal lamellar layers formed for thicker systems containing 6000 chains on a selective substrate, upon a heating/cooling cycle. This phase manifested the structural motifs favored by both the substrate and free surface simultaneously. The selective attraction provided by the bottom substrate induces horizontal lamella for the bottom layers, while the neutral character of the free surface favored a vertical lamella for the top layers. The same system could form a horizontal lamella phase or an island phase, the latter being favored by increasing the heating temperature and prolonging the heating/cooling ramp period, which allowed the system to undergo more drastic layer rearrangements. Overall, these results illustrate the tenet that the thin-film morphology can be controlled by both polymer/substrate chemistry (by tunning substrate selectivity and polymer surface tension) and processing variables (film thickness and duration/peak temperature of heating/cooling cycle).

The simple coarse-grained model used in this work captures the behavior of lamella thin film under laser annealing. It would be of interest to develop simulation models that would allow studying the other thin film morphologies, such as cylinder or gyroid phase, by applying an asymmetric dBCP chain. Also, a longer chain length model could be employed to study the effect of entanglement.

APPENDIX

∅ of the Final Structure at T_0 after 4×10^6 Step Heating/Cooling Ramp Period

The trends in the P2 values do not allow to fully detect the structural changes at the disordering temperature for the 4×10^6 steps heating/cooling, as this ramp period is long enough to allow the system to order back to a similar structure as the initial lamella phase. To circumvent this issue, we examine the ∅ values and the 2D structure factor color map to see whether the reformed lamella phase became uncorrelated from the initial phase.

Figure S1 shows the variation in the average alignment of end-to-end vectors, ∅ for each layer in the final structure obtained for the 4×10^6 steps heating/cooling. The results showed a small decrease of ∅ for all layers at around T* = 0.96, where the system starts to disorder, similar to the trends observed in P2. The fully disordering transition occurred at T'_{ODT} = 1.11, where ∅ decreases below 0.5, showing that the final structure is aligned along a different direction to that of the initial lamella phase, which can also be seen in the 2D structure factor (Figure S2).

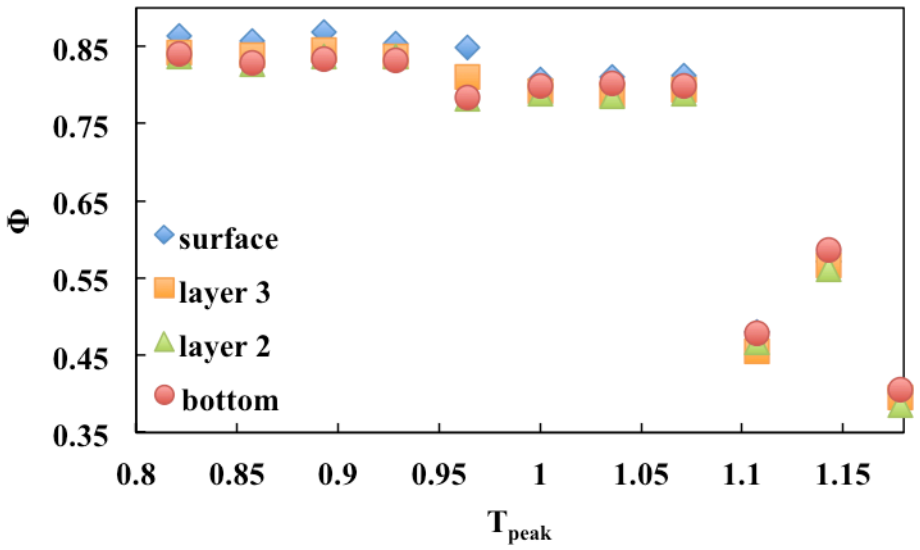

Figure S1. Order parameter Ø of the final structure at T_0 after 4×10^6 step heating/cooling ramp period as a function of peak heating temperature. System has 3000 chains.

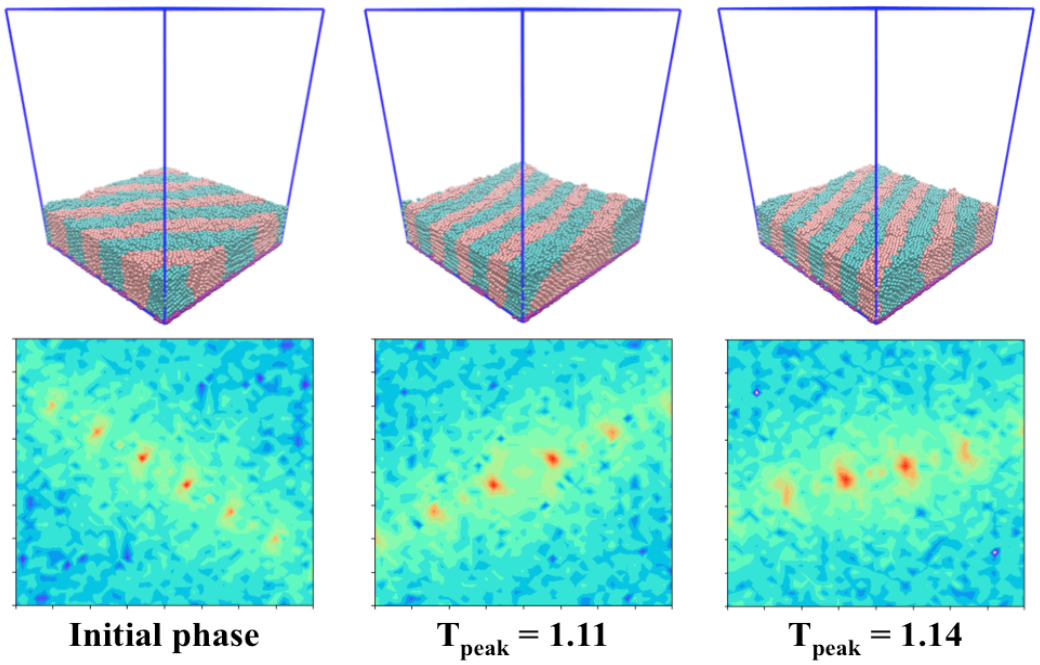

Figure S2. Selected snapshot and 2D structure factor for the initial phase and for final structures after 4×10^6 step heating/cooling cycle at peak heating temperatures of 1.11 and 1.14, showing that the lamella orientation in the final structure is independent of that of the initial phase.

Reheating the Island Phase

To examine if the formation of islands could be reduced or eliminated, the island phase formed at T_{peak} = 1.18 was heated to different T_{peak} values and cooled back to T_0 = 0.36, with 10^6 steps per ramp. Figure S3 shows a summary of these results including a comparison to the results from 10^6 step heating/cooling of the initial disordered system. The roughness of the reheated system reached a consistent *RP* value around 60, showing that the previously formed islands were hard to eliminate once established.

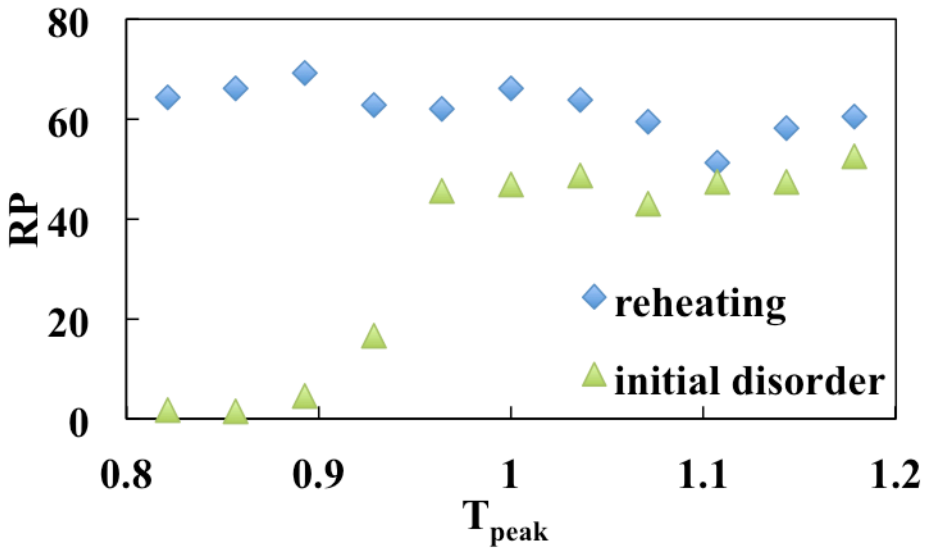

Figure S3. Roughness parameter for an initially disordered system and for island system at T_0 after reheating, the reheated system exhibited a nearly invariant roughness due to the persistence of the original islands.

Height Color Map of Island Phase

To visualize the height difference (i.e., the roughness) of island phase, we plot the height color map for each system. Figure S4 and S5 showed the effect of heating temperature and heating/cooling period to the formation of island phase respectively.

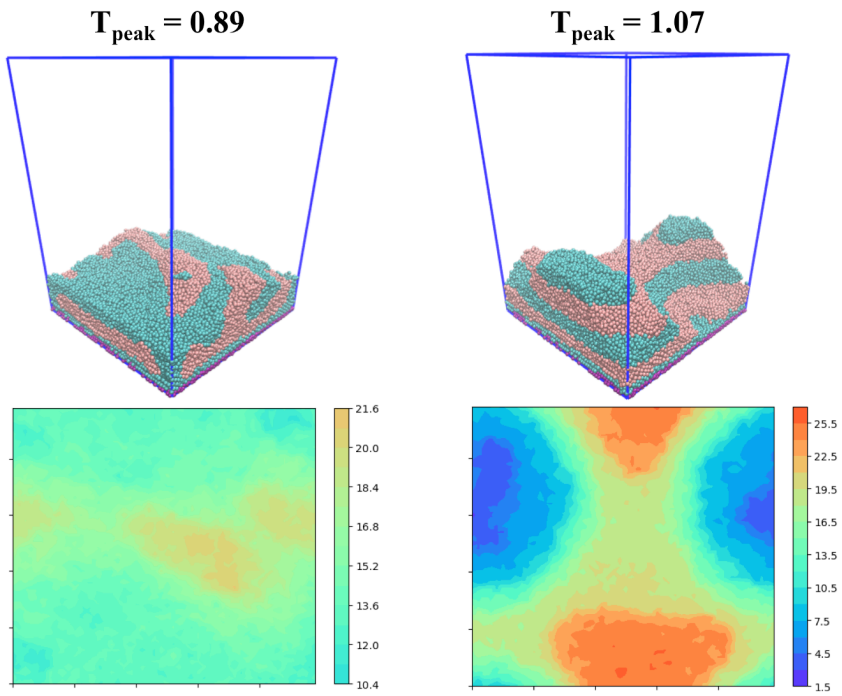

Figure S4. Snapshot and height map showing effect of higher heating temperature on the formation of islands.

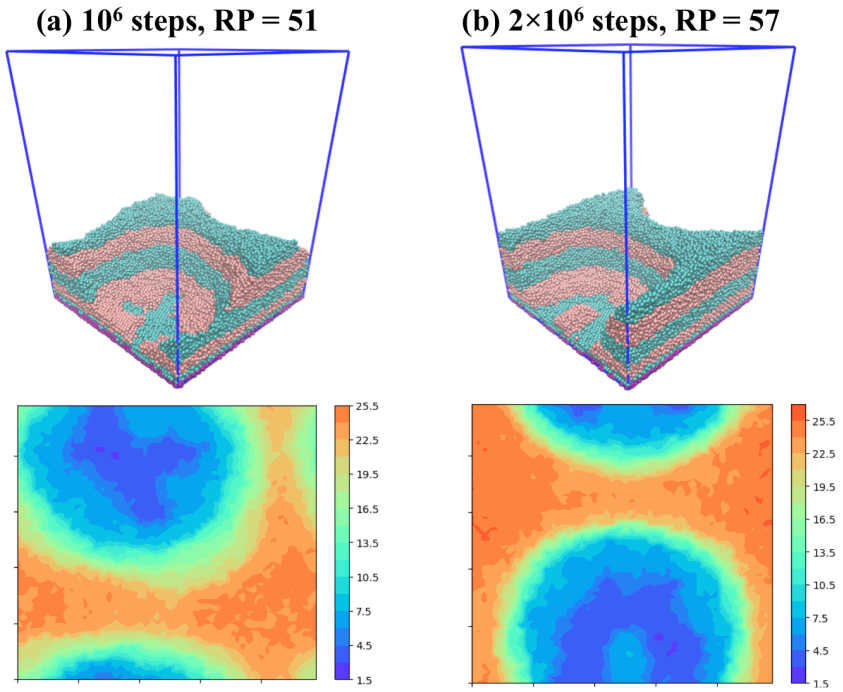

Figure S5. Snapshot and height map for island phase formed at T_{peak} = 1.18 under different heating/cooling periods.

REFERENCES

[1] Fredrickson, G. H., & Bates, F. S. (1996). Dynamics of Block Copolymers: Theory and Experiment. *Annual Review of Materials Science*, 26(1), 501–550.

[2] Bates, F. S. (1991). Polymer-Polymer Phase Behavior. *Science*, 251(4996), 898–905.

[3] Muthukumar, M., Ober, C. K., & Thomas, E. L. (1997). Competing interactions and levels of ordering in self- organizing polymeric materials. *Science*, 277(5330), 1225–1232.

[4] Bates, C. M., Maher, M. J., Janes, D. W., Ellison, C. J., & Willson, C. G. (2014). Block copolymer lithography. *Macromolecules*, 47(1), 2–12.

[5] Hellwig, O., Bosworth, J. K., Dobisz, E., Kercher, D., Hauet, T., Zeltzer, G., … Ruiz, R. (2010). Bit patterned media based on block copolymer directed assembly with narrow magnetic switching field distribution. *Applied Physics Letters*, 96(5), 1–4.

[6] Dorin, R. M., Phillip, W. A., Sai, H., Werner, J., Elimelech, M., & Wiesner, U. (2014). Designing block copolymer architectures for targeted membrane performance. *Polymer (United Kingdom)*, 55(1), 347–353.

[7] Meier-Haack, J., Taeger, A., Vogel, C., Schlenstedt, K., Lenk, W., & Lehmann, D. (2005). Membranes from sulfonated block copolymers for use in fuel cells. *Separation and Purification Technology*, 41(3), 207–220.

[8] Guo, X. D., Tan, J. P. K., Kim, S. H., Zhang, L. J., Zhang, Y., Hedrick, J. L., … Qian, Y. (2009). Computational studies on self-assembled paclitaxel structures:

Templates for hierarchical block copolymer assemblies and sustained drug release. *Biomaterials*, 30(33), 6556–6563.

[9] Rastogi, A. K., & St Pierre, L. E. (1969). Interfacial phenomena in macromolecular systems. *Journal of Colloid and Interface Science*, 31(2), 168–175.

[10] Mogi, Y., Nomura, M., Kotsuji, H., Ohnishi, K., Matsushita, Y., & Noda, I. (1994). Superlattice Structures in Morphologies of the ABC Triblock Copolymers. *Macromolecules*, 27(23), 6755–6760.

[11] Chremos, A., Nikoubashman, A., & Panagiotopoulos, A. Z. (2014). Flory-Huggins parameter χ, from binary mixtures of Lennard-Jones particles to block copolymer melts. *Journal of Chemical Physics*, 140(5), 1–10.

[12] Fredrickson, G. H., & Bates, F. S. (1996). Dynamics of Block Copolymers: Theory and Experiment. *Annual Review of Materials Science*, 26(1), 501–550.

[13] Matsen, M. W., & Bates, F. S. (1996). Unifying weak- and strong-segregation block copolymer theories. *Macromolecules*, 29(4), 1091–1098.

[14] Hu, H., Gopinadhan, M., & Osuji, C. O. (2014). Directed self-assembly of block copolymers: a tutorial review of strategies for enabling nanotechnology with soft matter. *Soft Matter*, 10(22), 3867.

[15] Darling, S. B. (2007). Directing the self-assembly of block copolymers. *Progress in Polymer Science (Oxford)*, 32(10), 1152–1204.

[16] Albert, J. N. L., & Epps, T. H. (2010). Self-assembly of block copolymer thin films. *Materials Today*, 13(6), 24–33.

[17] Li, Y., & Kaito, A. (2006). Highly oriented structure formed in a lamella-forming diblock copolymer with high molar mass. *European Polymer Journal*, 42(9), 1986–1993.

[18] Zhang, J., Posselt, D., Smilgies, D. M., Perlich, J., Kyriakos, K., Jaksch, S., & Papadakis, C. M. (2014). Lamellar diblock copolymer thin films during solvent vapor annealing studied by gisaxs: Different behavior of parallel and perpendicular lamellae. *Macromolecules*, 47(16), 5711–5718.

[19] Rockford, L., Liu, Y., Mansky, P., Russell, T. P., Yoon, M., & Mochrie, S. G. J. (1999). Polymers on nanoperiodic, heterogeneous surfaces. *Physical Review Letters*, 82(12), 2602–2605.

[20] Jacobs, A. G., Jung, B., Ober, C. K., & Thompson, M. O. (2014). Control of PS-b-PMMA directed self-assembly registration by laser induced millisecond thermal annealing. *Proc. SPIE*, 9049, 90492B–90492B–7.

[21] Jacobs, A. G., Liedel, C., Peng, H., Wang, L., Smilgies, D.-M., Ober, C. K., & Thompson, M. O. (2016). Kinetics of Block Copolymer Phase Segregation during Sub-millisecond Transient Thermal Annealing. Macromolecules, 49(17), 6462–6470.

[22] Papakonstantopoulos, G. J., Daoulas, K. C., Muller, M., & de Pablo, J. J. (2016). Monte Carlo simulation study of diblock copolymer self assembly. *arXiv preprint* arXiv:1604.05265

[23] Arya, G., Rottler, J., Panagiotopoulos, A. Z., Srolovitz, D. J., & Chaikin, P. M. (2005). Shear ordering in thin films of spherical block copolymer. *Langmuir*, 21(24), 11518–11527.

[24] Morita, H., Tanaka, K., Kajiyama, T., Nishi, T., & Doi, M. (2006). Study of the glass transition temperature of polymer surface by coarse-grained molecular dynamics simulation. *Macromolecules*, 39(18), 6233–6237.

[25] Paeng, K., Swallen, S. F., & Ediger, M. D. (2011). Direct measurement of molecular motion in freestanding polystyrene thin films. *Journal of the American Chemical Society*, 133(22), 8444–8447.

[26] Forrey, C., Yager, K. G., & Broadaway, S. P. (2011). Molecular Dynamics Study of the Role of the Free Surface on Block Copolymer Thin Film Morphology and Alignment, *ACS Nano*(4), 2895–2907.

[27] Yager, K. G., Forrey, C., Singh, G., Satija, S. K., Page, K. A., Patton, D. L., … Karim, A. (2015). Thermally-induced transition of lamellae orientation in block-copolymer films on "neutral" nanoparticle-coated substrates. *Soft Matter*, 11(25), 5154–5167.

[28] Grest, G. S., Lacasse, M., Kremer, K., & Gupta, A. M. (1996). Efficient continuum model for simulating polymer blends and copolymers. *The Journal of Chemical Physics*, 105(23), 10583–10594.

[29] J. D. Weeks, D. Chandler and H. C. Andersen. Role of repulsive forces in determining the equilibrium structure of simple liquids. *The Journal of Chemical Physics*, 54, 5237-5247 (1971).

[30] Plimpton, S., Pollock, R., & Stevens, M. J. (1997). Particle Mesh Ewald and rRESPA for Parallel Molecular Dynamics Simulations. *Proceedings of the Eighth Siam Conference on Parallel Processing for Scientific Computing*, 1–13.

[31] Humphrey, W., Dalke, A., & Schulten, K. (1996). Visual molecular dynamics. *Journal of Molecular Graphics*, 14(1), 33–38.

[32] Murat, M., Grest, G. S., & Kremer, K. (1999). Statics and Dynamics of Symmetric Diblock Copolymers: A Molecular Dynamics Study. *Macromolecules*, 32, 595–609.

[33] John, B. S., Juhlin, C., & Escobedo, F. A. (2008). Phase behavior of colloidal hard perfect tetragonal parallelepipeds. *Journal of Chemical Physics*, 128(4).

[34] Zheng, Z., Liu, H., Shen, J., Liu, J., Wu, Y., & Zhang, L. (2016). Tailoring the Static and Dynamic Mechanical Properties of Tri-Block Copolymers through Molecular Dynamics Simulation. *Polymers*, 8(9), 335.

[35] Zhang, K. (2016). On the Concept of Static Structure Factor. *arXiv preprint* arXiv:1606.03610.

[36] Suh, H. S., Kang, H., Nealey, P. F., & Char, K. (2010). Thickness dependence of neutral parameter windows for perpendicularly oriented block copolymer thin films. *Macromolecules*, 43(10), 4744–4751.

[37] Peters, R. D., Yang, X. M., Kim, T. K., & Nealey, P. F. (2000). Wetting behavior of block copolymers on self-assembled films of alkylchlorosiloxanes: Effect of grafting density. *Langmuir*, 16(24), 9620–9626.

[38] Maher, M. J., Self, J. L., Stasiak, P., Blachut, G., Ellison, C. J., Matsen, M. W., Bates, C. M., Willson, C. G. (2016). Structure, Stability, and Reorganization of 0.5 L0Topography in Block Copolymer Thin Films. *ACS Nano*, 10(11), 10152–10160.

[39] Fasolka, M. J., & Mayes, A. M. (2001). Block Copolymer Thin Films: Physics and Applications. *Annual Review of Materials Research*, 31(1), 323–355.

[40] Smith, A. P., Douglas, J. F., Meredith, J. C., Amis, E. J., & Karim, A. (2001). Combinatorial study of surface pattern formation in thin block copolymer films. *Physical Review Letters*, 87(1), 4–7.

[41] Pickett, G. T., & Balazs, A. C. (1997). Equilibrium Orientation of Confined Diblock Copolymer Films. *Macromolecules*, 30(10), 3097–3103.

[42] Heier, J., Kramer, E. J., Groenewold, J., & Fredrickson, G. H. (2000). Kinetics of individual block copolymer island formation and disappearance near an absorbing boundary. *Macromolecules*, 33(16), 6060–6067.

[43] Green, P. F., & Limary, R. (2001). Block copolymer thin films: pattern formation and phase behavior. *Advances in Colloid and Interface Science*, 94(1–3), 53–81.

[44] Zhang, X., Berry, B. C., Yager, K. G., Kim, S., Jones, R. L., Satija, S., … Karim, A. (2008). Surface Morphology Diagram for Cylinder-Forming Block Copolymer Thin Films. *ACS Nano*, 2(11), 2331–2341.

[45] Ponsinet, V. (2015). Nanopatterns produced by directed self-assembly in block copolymer thin films. *Polymer Surfaces in Motion* (pp. 73-97). Springer, Cham.

[46] Kim, E., Choi, S., Guo, R., Ryu, D. Y., Hawker, C. J., & Russell, T. P. (2010). Transition behavior of PS-b-PMMA films on the balanced interfacial interactions. *Polymer*, *51*(26), 6313-6318.

[47] Croll, A. B., Matsen, M. W., Shi, A. C., & Dalnoki-Veress, K. (2008). Kinetics of layer hopping in a diblock copolymer lamellar phase. *The European Physical Journal E*, *27*(4), 407-411.

[48] Cross, M. M. (1979). Relation between viscoelasticity and shear-thinning behaviour in liquids. *Rheologica Acta*, 18(5), 609-614.

[49] Vladkov, M., & Barrat, J. L. (2006). Linear and nonlinear viscoelasticity of a model unentangled polymer melt: molecular dynamics and rouse modes analysis. *Macromolecular theory and simulations*, *15*(3), 252-262.

[50] Patterson, G. D., Carroll, P. J., & Stevens, J. R. (1983). Photon correlation spectroscopy of polystyrene as a function of temperature and pressure. *Journal of Polymer Science Part B: Polymer Physics*, *21*(4), 605-611.

[51] Isayev, A. I. (1987). *Injection and compression molding fundamentals*. New York: Dekker.